European Journal of Medicinal Chemistry 252 (2023) 115289

Contents lists available at ScienceDirect

European Journal of Medicinal Chemistry

journal homepage: www.elsevier.com/locate/ejmech

Research paper

Novel *O*-benzylcinnamic acid derivative L26 treats acute lung injury in mice by MD-2

Xiang Li [a,b,1], Lina Yin [c,1], Jing Liao [a,1], Jun Yang [a], Binhao Cai [a], Yiming Yu [a], Sijia Su [a], Zhiteng Du [a], Xiaobo Li [a], Ying Zhou [a], Pan Chen [a,d], Won-Jea Cho [d], Nipon Chattipakorn [e], Aleksandr V. Samorodov [f], Valentin N. Pavlov [f], Fengzhi Zhang [a,***], Guang Liang [a,b,c,**], Qidong Tang [a,b,*]

[a] *Chemical Biology Research Center, School of Pharmaceutical Sciences, Wenzhou Medical University, Wenzhou, 325035, Zhejiang, China*
[b] *Wenzhou Institute, University of Chinese Academy of Sciences, Wenzhou, 325024, Zhejiang, China*
[c] *School of Pharmacy, Hangzhou Medical College, Hangzhou, 311399, Zhejiang, China*
[d] *College of Pharmacy, Chonnam National University, Gwangju, 61186, South Korea*
[e] *Cardiac Electrophysiology Research and Training Center, Faculty of Medicine, Chiang Mai University, Chiang Mai, 50200, Thailand*
[f] *Department of Pharmacology, Bashkir State Medical University, Ufa City, 450005, Russia*

ARTICLE INFO

Keywords:
Acute lung injury
Cinnamic acid derivatives
Myeloid differentiation 2
Inflammation

ABSTRACT

Acute lung injury (ALI) is an inflammation-mediated respiratory disease that is associated with a high mortality rate. In this study, a series of novel *O*-benzylcinnamic acid derivatives were designed and synthesized using cinnamic acid as the lead compound. We tested the preliminary anti-inflammatory activity of the compounds by evaluating their effect on inhibiting the activity of alkaline phosphatase (ALP) in Hek-Blue-TLR4 cells, in which compound **L26** showed the best activity and 7-fold more active than CIN. ELISA, immunoprecipitation, and molecular docking indicated that **L26** targeted MD-2 protein and competed with LPS to bind to MD-2, which resulted in the inhibition of inflammation. In the LPS-induced mouse model of ALI, **L26** was found to decrease ALP activity and inflammatory cytokine TNF-α release to reduce lung injury by inhibiting the NF-κB signaling pathway. Acute toxicity experiments showed that high doses of **L26** did not cause adverse reactions in mice, and it was safe *in vivo*. Also, the preliminary pharmacokinetic parameters of **L26** were investigated in SD rats ($T_{1/2}$ = 4.246 h). In summary, **L26** exhibited optimal pharmacodynamic and pharmacokinetic characteristics, which suggested that **L26** could serve as a potential agent for the development of ALI treatment.

1. Introduction

Inflammation is the process that protects the tissues from exogenous pathogens and repairs the body upon infection or trauma. However, the infiltration of a mass of inflammatory cells produces excess pro-inflammatory factors such as TNF-α, and IL-6 [1]. Additionally, if the inflammatory response is amplified and uncontrolled, it could cause various diseases, such as bacterial pneumonia and Acute lung injury [2]. ALI is a respiratory disease with a greater than 40% mortality rate [3]. ALI causes systemic inflammation and is characterized by pulmonary infiltrates, edema and hypoxemia. Supportive therapy combined with medication-assisted therapy has been the conventional treatment modality used to cure ALI [4–7]. However, the widespread application of the above treatment is hindered due to the limited availability of relevant equipment in clinical practice [8,9]. There is a lack of effective drugs that could significantly reduce mortality and improve the quality of life of ALI patients [10–13]. Therefore, there is an urgent need to develop targeted therapeutics for the clinical treatment of ALI.

Excessive inflammation caused by endotoxins is one of the leading causes of ALI [14–16]. Lipopolysaccharide (LPS) is a type of endotoxin, and toll-like receptor 4 (TLR4) is the receptor for LPS [17,18]. After the activation of TLR4 by LPS, an inflammatory cascade is initiated by

* Corresponding author. Chemical Biology Research Center, School of Pharmaceutical Sciences, Wenzhou Medical University, Wenzhou, 325035, Zhejiang, China.
** Corresponding author. Chemical Biology Research Center, School of Pharmaceutical Sciences, Wenzhou Medical University, Wenzhou, 325035, Zhejiang, China.
*** Corresponding author.
E-mail addresses: zhangfengzhi@zjut.edu.cn (F. Zhang), wzmcliangguang@163.com (G. Liang), tangqidongcn@126.com (Q. Tang).
[1] These authors contribute equally to this work.

https://doi.org/10.1016/j.ejmech.2023.115289
Received 27 January 2023; Received in revised form 7 March 2023; Accepted 14 March 2023
Available online 17 March 2023

leading to the release of alarm signals, which trigger the nuclear factor-κB (NF-κB) pathway and induce inflammation [19]. The Myeloid differentiation protein-2 (MD-2) plays a critical role in this process, MD-2 and TLR4 form the MD-2/TLR4 complex on the cell membrane. In the absence of agonists, the TLR4/MD-2 complex is in equilibrium between monomers and dimers. Upon CD14-mediated transfer of LPS to MD-2, TLR4/MD-2 complex dimerization occurs [20,21]. According to the published crystal structure of MD-2 protein, it is a globulin formed by two anti-parallel β sheets, shaping a sizeable hydrophobic pocket inside. The internal surface of the pocket is completely lined with hydrophobic residues to form an opening hydrophobic pocket, to which facilitating the binding of hydrophobic parts of LPS. Compounds containing strong hydrophobic structures could compete with LPS for this pocket [20,22]. Hence, it is an excellent strategy to inhibit the interaction between MD-2 protein and LPS to suppress inflammation mediated injury to the tissues and to successfully relieve clinical symptoms of ALI [23].

The development of new drugs from structurally complex natural products has enabled significant progress in medicine and accelerated drug research [24]. For example, morphine was isolated from opium resin and approved as a painkiller by the FDA owing to its superior analgesic properties [25] (Fig. 1). Camptothecin was developed as an antineoplastic agent because of its ability to inhibit type I DNA topoisomerase [26,27]. Besides, increasing number of studies have verified that retaining the active skeleton of natural products and making targeted modifications could generate compounds with better biological activity [24]. For instance, the hypoglycemic drug Metformin was obtained by replacing the 3-methylbutenyl group in Galegine with *N*, *N*-dimethylformamide [28], and another classical antipyretic analgesic aspirin was obtained by the acetylation of salicylic acid [29]. Cinnamic acid (CIN) is an organic acid extracted from cinnamon, possessing good anti-inflammatory activity [30–32]. Previously, we found that cinnamamide derivatives inhibited excessive inflammatory response by targeting the MD-2 protein [33]. Therefore, CIN was selected as the lead compound in this study to design further MD-2 inhibitors. Recently, Sang'et al. reported that the presence of *O*-alkyl groups at the para position of the phenyl ring improved the activity of CIN [32] (Fig. 2). Thus, we decided to introduce the *O*-benzyl group at the opposite position of CIN to increase its lipophilicity. Moreover, thiazole-2-amine, benzo[d]thiazol-2-amine, and benzo[d]imidazole-2-amine have been reported to have anti-inflammatory effects, and have been employed as pharmacophores in several marketed drugs, thus, we planned to introduce them into CIN [34–36]. Finally, we designed a series of *O*-benzyl CIN derivatives (Fig. 2).

In this study, the anti-inflammatory activity of compounds was measured by screening for inhibitory effects on the production of the ALP activity in Hek-Blue-TLR4 cells. The preferred compound (*E*)-*N*-(1*H*-benzo[d]imidazole-2-yl)-3-(4-(((3-methoxybenzyl)oxy)phenyl)aniline (**L26**) was found to reduce the expression of inflammatory factors by binding to MD-2 protein, and competitively antagonized LPS binding to MD-2. Furthermore, we established an LPS-induced mouse model of ALI to evaluate the anti-inflammatory effects of **L26** in *vivo* and tested the pharmacokinetics of **L26** in SD rats. The results indicated that **L26** attenuated LPS-induced lung inflammation by inhibiting the activation of NF-κB signaling pathway and displayed good pharmacokinetic parameters. In summary, the *in vitro* and *in vivo* results revealed that **L26** might serve as a potential therapeutic agent for the treatment of ALI.

2. Results and discussion

2.1. Chemistry

The synthetic pathways for all the target compounds are listed in Scheme 1, and the compounds were obtained in three steps. *P*-hydroxybenzaldehyde and various bromobenzyls were dissolved in acetonitrile (MeCN) and then potassium carbonate (K_2CO_3) was added to the mixture under nitrogen gas. After refluxing at 80 °C for 2 h, the intermediates **1a-1j** were obtained by classical nucleophilic substitution. The Perkin reaction was used to convert various benzaldehydes into their corresponding CINs. Intermediates **1a-1j** were dissolved in pyridine and mixed with 2 equivalents of malonic acid, and refluxed at high temperature for 4–6 h with piperidine as the catalyst to generate the different CIN derivatives **2a-2j**. Subsequently, various CINs were dissolved in dichloromethane with triethylamine. In the presence of *O*-(benzotriazol-1-yl)-*N*,*N*,*N*′,*N*′-tetramethyluronium tetrafluoroborate (TBTU), the cinnamic derivatives were generated from the condensation of acids with 2-aminothiazole, 2-aminobenzthiazole, or 2-aminobenzimidazole at room temperature, respectively, and the final target compounds **L1**-**L27** were purified using a chromatographic column. NMR spectroscopy, HPLC, and LC-MS spectrometry were used to characterize and confirm the structure of final products.

2.2. Biological evaluation

2.2.1. Assessment of anti-inflammatory activity and SAR of the compounds

The method proposed by Kata Tombácz's group to test the anti-inflammatory ability of compounds through alkaline phosphatase was used in this study [37]. Professor Cheng's articles published in *Eur. J. Med. Chem.* and *J. Med. Chem.* also adopted this method [38,39]. Human TLR4, MD-2, and CD14 co-receptor genes, as well as the secreted embryonic alkaline phosphatase gene (SEAP), were co-transfected into HEK293 cells to generate Hek-blue-TLR4 cells [40]. The SEAP signaling is induced by the NF-κB signaling pathway, which was activates by LPS mediated TLR4 signaling [37]. When the SEAP signal was activated, ALP

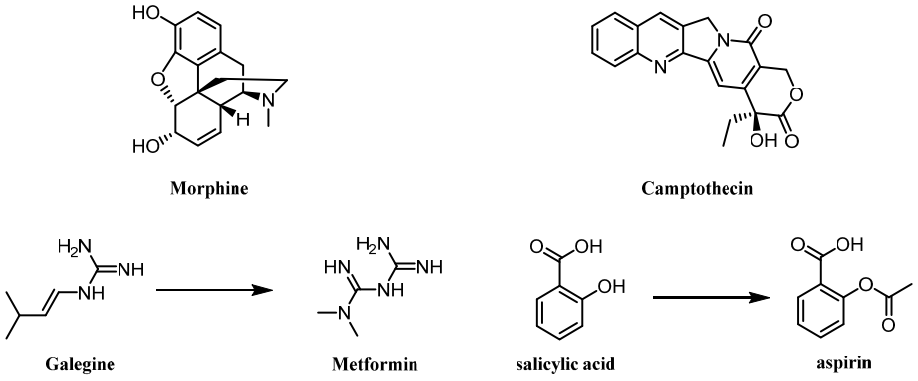

Fig. 1. Clinical drugs were developed from natural products.

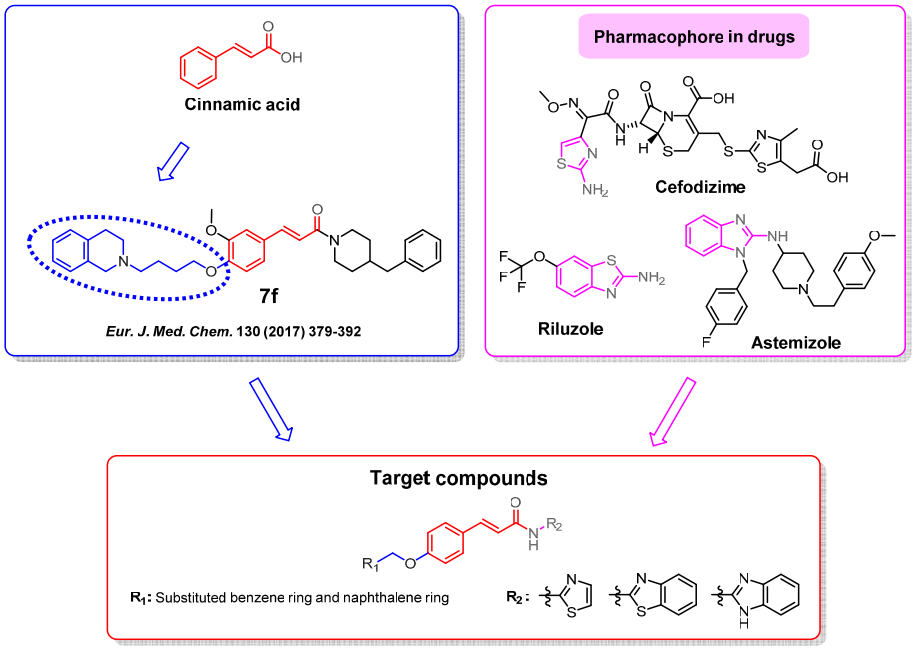

Fig. 2. Design strategy for *O*-benzyl cinnamic acid derivatives.

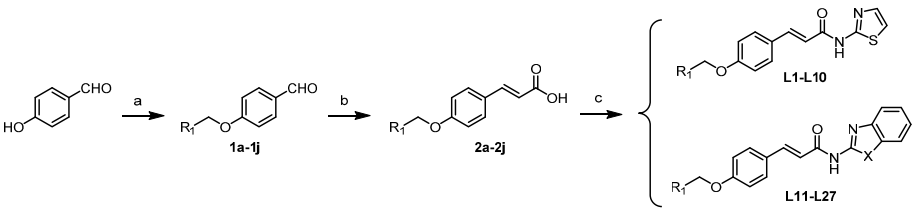

L1: R_1 = 3-methylphenyl
L2: R_1 = 4-methylphenyl
L3: R_1 = 4-Isopropphenyl
L4: R_1 = 3-fluorophenyl
L5: R_1 = 4-fluorophenyl
L6: R_1 = 3-methoxyphenyl
L7: R_1 = 4-methoxyphenyl
L8: R_1 = 2,6-dichlorinephenyl
L9: R_1 = 3-chlorinphenyl
L10: R_1 = naphthalene-2-yl
L11: R_1 = 3-methylphenyl, X = S
L12: R_1 = 4-methylphenyl, X = S
L13: R_1 = 4-Isopropphenyl, X = S
L14: R_1 = 3-fluorophenyl, X = S
L15: R_1 = 4-fluorophenyl, X = S
L16: R_1 = 3-methoxyphenyl, X = S
L17: R_1 = 4-methoxyphenyl, X = S
L18: R_1 = 2,6-dichlorinephenyl, X = S
L19: R_1 = 3-chlorinphenyl, X = S
L20: R_1 = naphthalene-2-yl, X = S
L21: R_1 = 4-methylphenyl, X = N
L22: R_1 = 3-fluorophenyl, X = N
L23: R1 = 4-fluorophenyl, X = N
L24: R_1 = 2,6-chlorinephenyl, X = N
L25: R_1 = 3-chlorinphenyl, X = N
L26: R_1 = 3-methoxyphenyl, X = N
L27: R_1 = naphthalene, X = N

Scheme 1. Reagents and conditions: (a) various benzyl bromide, MeCN, K_2CO_3, 80 °C; (b) pyridine, piperidine, propanedioic acid, 110 °C; (c) 1*H*-benzo[d]imidazole-2-amine, benzo[d]thiazol-2-amine, aminothiazole, TBTU, dichloromethane, rt.

was released in large quantities, and its expression was positively correlated with the secretion of pro-inflammatory cytokines [37]. The anti-inflammatory activity of the synthetic compounds was measured by evaluating the inhibition of ALP activity in Hek-blue-TLR4 cells. Although the tested results for activity seem weak (high on IC_{50} value or low on inhibition rate, such as the IC_{50} value of 12.45 μM for the optimal compound **8a** in *Eur. J. Med. Chem.* 154 (2018) 253–266), this method is sensitive and rapid for detecting anti-inflammatory factors, and we want to promote this method in this study.

As shown in Table 1, the activity of more than half of the compounds was greater than that of CIN, and the activity of most potent compound **L26** was 7-fold greater than that of CIN, which proved the correctness of the design strategy of the target compounds. The preliminary structure-activity relationship (SAR) analysis indicated that the compounds that possessed benzimidazole groups, had higher rate of inhibition of ALP activity in comparison to the compounds that possessed thiazole or benzothiazole groups. Some compounds that possessed benzimidazole group showed excellent inhibition activities, such as **L21**, **L22**, **L25,** and **L26** (43.08%, 55.45%, 41.13%, and 64.30%, respectively). The compounds **L21**-**L27** were selected for further SAR analysis on the R_1 position. The activities of the remaining compounds with the benzyl substitution in R_1 position were more potent than those with naphthalene substitutions (**L27**). Moreover, the activity of meta-substituted compounds was significantly better than that of the para-substituted compounds (**L22** vs **L23**), and the contribution of the electron-donating effect of meta-substituted groups to activity was significantly higher than that of the electron-withdrawing groups (**L25** vs **L26**). In addition, the presence of more electron-withdrawing groups on the benzene ring significantly decreased the inhibition of ALP activity (**L24** vs **L25**). As shown in Fig. S1, excluding compound **L22**, these compounds showed no significant toxicity in Hek-blue-TLR4 cells after 24 h treatment (cell variability >80%). Therefore, **L26** was selected as the hit compound for further study.

In addition to the above-mentioned method of detecting ALP to test the anti-inflammatory activity of the compound, we also used ELISA assay to further confirm the anti-inflammatory activity. To determine

Table 1
The structure and inhibitory activity against alkaline phosphatase for compounds **L1**-**L27**.

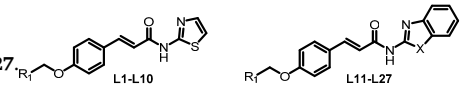

Compound	R_1	X	Inhibition[a] (%, 10 μM)
L1	3-methylphenyl	–	2.28 ± 0.41
L2	4-methylphenyl	–	15.31 ± 1.12
L3	4-Isopropphenyl	–	NA[b]
L4	3-fluorophenyl	–	7.66 ± 0.44
L5	4-fluorophenyl	–	12.05 ± 1.58
L6	3-methoxyphenyl	–	NA
L7	4-methoxyphenyl	–	NA
L8	2,6-dichlorinephenyl	–	8.16 ± 1.41
L9	3-chlorinphenyl	–	NA
L10	naphthalene-2-yl	–	3.63 ± 0.91
L11	3-methylphenyl	S	9.26 ± 0.67
L12	4-methylphenyl	S	NA
L13	4-Isopropphenyl	S	14.04 ± 0.57
L14	3-fluorophenyl	S	19.00 ± 2.66
L15	4-fluorophenyl	S	12.84 ± 0.63
L16	3-methoxyphenyl	S	14.12 ± 0.34
L17	4-methoxyphenyl	S	16.39 ± 0.58
L18	2,6-dichlorinepheny	S	11.99 ± 2.49
L19	3-chlorinphenyl	S	NA
L20	naphthalene-2-yl	S	14.17 ± 1.06
L21	4-methylphenyl	N	43.08 ± 0.63
L22	3-fluorophenyl	N	55.45 ± 3.38
L23	4-fluorophenyl	N	29.65 ± 5.83
L24	2,6-chlorinephenyl	N	19.64 ± 2.99
L25	3-chlorinphenyl	N	41.13 ± 2.63
L26	3-methoxyphenyl	N	64.30 ± 3.38
L27	naphthalene	N	9.07 ± 0.25
CIN			9.51 ± 1.42

[a] Data shown as mean ± SEM of three independent experiments.
[b] Exhibited no effect.

the IC_{50} of the best compound identified by Elisa assay is a favorable method for evaluating the ability of the compound to inhibit pro-inflammatory factors, such as IL-6 and TNF-α. We have used this approach in our previous articles published in *Eur. J. Med. Chem.* and *J. Med. Chem.* [41,42]. Accordingly, we evaluated the anti-inflammatory activity of **L26** in LPS-induced RAW 264.7 macrophages. The results confirmed that **L26** suppressed the expression of IL-6 and TNF-α in RAW 264.7 cells in a concentration-dependent manner. (IL-6: IC_{50} = 2.58 μM, TNF-α: IC_{50} = 8.41 μM, Fig. 3).

2.2.2. *Compound **L26** inhibits LPS-induced inflammation and directly targets MD-2*

MD-2 is known to be involved in the cellular recognition of LPS by TLR4, the dimerization of TLR4 is triggered by the MD-2/LPS complex, and then the MD-2/LPS/TLR4 complex activates the NF-κB signaling pathway to generate inflammatory cytokines [20]. Our findings from previous studies found that cinnamamide derivatives targeted MD-2 protein and blocked the binding of LPS to TLR4, thereby reducing cellular inflammation [33]. As **L26** was a new cinnamamide/cinnamic derivative, we aimed to verify whether **L26** targeted on MD-2 protein. Firstly, MD-2 protein was pre-mixed with Biotin-labeled LPS for 1 h and then it was incubated with or without **L26**, and the absorbance was measured. The results suggested that **L26** competitively inhibited the binding of LPS to MD-2, which proved that **L26** could bind to MD-2 at molecular level (Fig. 4A). Subsequently, we conducted an immunoprecipitation experiment at cellular level. After pre-treatment with **L26**, the experimental results showed that **L26** prevented the formation of LPS/MD-2/TLR4 polymers in RAW264.7 cells, indicating that **L26** targeted on MD-2 protein, thereby exhibiting good anti-inflammatory activity (Fig. 4B).

2.2.3. *Molecular docking analysis of **L26** with MD-2*

The findings from the above biological experiments showed that **L26** suppressed inflammation by directly targeting the interaction of MD-2 protein with LPS. High-resolution MD-2 crystals isolated from human TLR4/MD-2 complexed (Protein Data Bank ID: 4G8A) docked with **L26**. The results showed that the *O*-benzyl group of **L26** was fully extended into the hydrophobic pocket of MD-2. Meanwhile, the benzimidazole moiety of **L26** was exposed toward the solvent region (Fig. 5A). Fig. 5B illustrates the interaction between **L26** and the active sites of MD-2, and that the benzimidazole group provides the hydrogen-bond donors and forms hydrogen bond with the CYC-133 residue. Simultaneously, the middle benzene ring was stacked with PHE-151 to form the π-π interaction (Fig. 5B), and the docking score was −7.99 kcal/mol.

2.2.4. *Compound **L26** attenuates LPS-induced ALI in mice*

To further evaluate the anti-inflammatory effect of **L26** *in vivo*, we administered the mice (C57BL/6) with **L26** (5 mg/kg) intra-gastrically. Then LPS was injected into the trachea of the mice to induce ALI. 6 h later, the mice were sacrificed. ALI is known to be an inflammatory syndrome and TNF-α is the vital inflammatory mediator in the progression of ALI [43]. Thus, we tested the inflammatory responses of bronchoalveolar lavage fluid (BALF) and serum to TNF-α. As shown in Fig. 6A, B and 6C, compared with the LPS group and the CIN group, the expression of TNF-α in the treatment group was significantly lower. **L26** also notably downregulated the expression of pro-inflammatory factor mRNA, suggesting that **L26** alleviated the inflammation associated with ALI. In addition to TNF-α, ALP is also known as a reliable indicator of the impact of chemical reagents on the animal lungs [44]. As shown in Fig. 6D, LPS-induced expression of ALP was notably upregulated in BALF, while **L26** could inhibit these effects, confirming the anti-inflammatory effect of **L26**. We also detected the total protein concentration in BALF. In addition to the control group, the total protein concentration in the BALF of mice treated with LPS was significantly

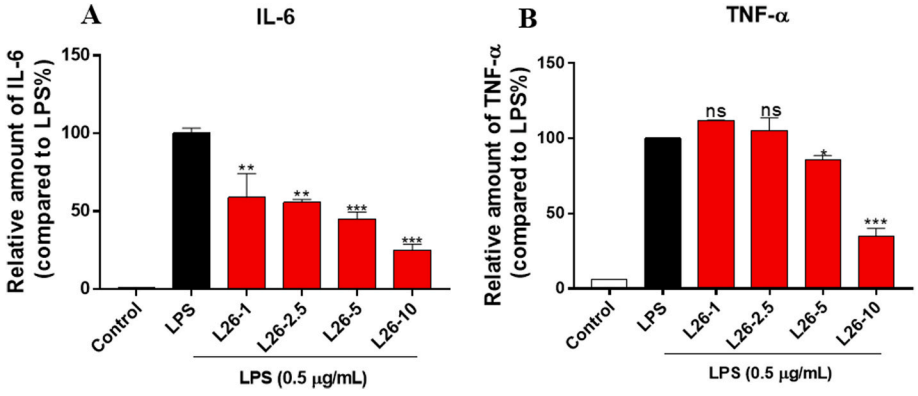

Fig. 3. **L26** inhibitory effects on the production of the pro-inflammatory cytokines TNF-α and IL-6 in a dose-dependent manner. RAW 264.7 cells were pre-treated with CIN (10 μM), vehicle control (DMSO) or different concentrations of **L26** ranging from 1 to 10 μM for 30 min before LPS treatment (0.5 μg/mL). 24 h later, we collected and transferred 30 μL sample buffer from each well of the cell culture plate to a transparent 96-well plate. According to the manufacturer's instructions, the absorbance (OD) values were measured by a plate reader, and the mean ± SEM values in triplicates were reported as the percentage of the values for the LPS group; *P < 0.05, **P < 0.001 compared to the LPS group, calculated by student's t-test.

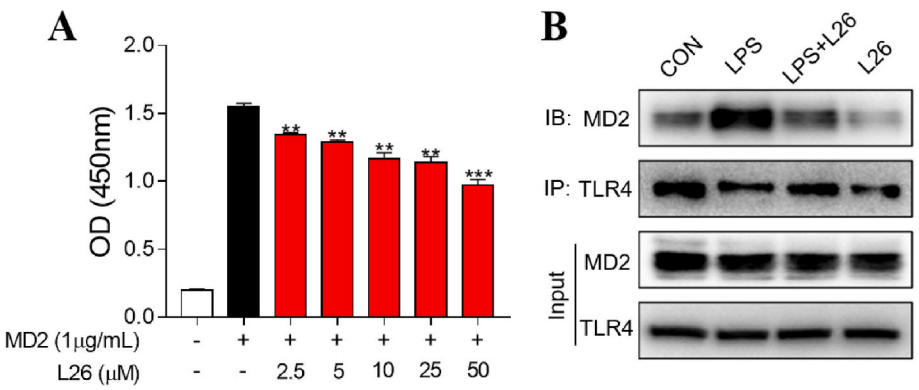

Fig. 4. Evaluation of the binding affinity of **L26** for MD-2 by ELISA, and co-immunoprecipitation. (A) Determination of the binding of LPS to MD-2 in the presence of **L26** by ELISA. (B) Evaluation of the effects of **L26** on LPS-induced TLR4-MD-2 complex dimerization in RAW 264.7 macrophages using co-immunoprecipitation. The mean ± SEM values in triplicates were reported as the percentage of the values for the LPS group; *P < 0.05, **P < 0.001 compared to the LPS group, calculated by student's t-test.

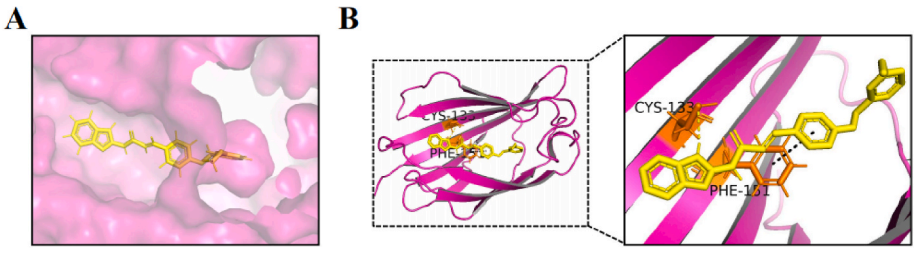

Fig. 5. Analysis of the interaction between **L26** and MD-2 by molecular docking. (A, B) AutoDock Tools 4.2 was used to perform the molecular docking of **L26** with rhMD-2 (PDB 4G8A). Yellow and black dashed lines are hydrogen bonds and π-π stacking interactions, respectively.

elevated, which could be rescued by **L26** (Fig. 6E).

An extensive collection of clinical data has suggested that pulmonary vascular permeability increased during ALI, leading to pulmonary edema [45]. Therefore, we evaluated the wet/dry weight ratio of the mice lungs (Fig. 6F), and the results for the administration group were significantly better than the model group and the positive drug group. Based on previous study, neutrophils and macrophages were reported to be recruited into the infected lung tissue to control the infection. But under pathological conditions, large amounts of inflammatory cells are known to infiltrate and produce inflammatory factors, damage the lung epithelial cells, and cause interstitial edema, congestion, and alveolar septum thickening [46] (Fig. 6G). To further evaluate the anti-inflammatory effects of **L26**, we performed the histological evaluation of the lung tissue from the mice, which showed that **L26** effectively alleviated the pathological changes associated with ALI (Fig. 6H). The above findings effectively indicated that **L26** had an excellent anti-inflammatory effect *in vivo*.

2.2.5. *L26 inhibits NF-κB signaling in vivo*

It is well known that LPS induces the dimerization of TLR4 and regulates multiple downstream signaling pathways [17]. Besides, NF-κB signaling pathway has been associated with the development of ALI [43]. To determine how **L26** suppressed LPS-induced lung damage, we investigated whether **L26** inhibited the NF-κB pathway in the lung tissue. As illustrated in Fig. 7, **L26** significantly inhibited the phosphorylation of p65 and increased the release of IκB-α. The above results indicated that **L26** exerted anti-inflammatory effect *in vivo* by restraining the NF-κB signaling pathway.

2.2.6. *Evaluation of the acute toxicity of compound L26 to ICR mice*

Further acute toxicity studies were required in order further to evaluate the safety of compound **L26** *in vivo*. Mice received intragastric compound **L26** on the first day at a dosage of 1000 and 1500 mg/kg, respectively. The body weight of each mouse was recorded every other day for 10 consecutive days, untreated mice were used as the control group, and their weight was taken as a reference. There were no deaths or drug-related serious adverse events in any experimental groups during the experiment. As shown in Fig. 8, the body weight of the three groups of mice increased steadily every day, and there was no significant statistical difference between the control and experiment groups. After the last observation period, the mice were sacrificed and organs were dissected for HE staining experiments. It can be seen from Fig. 9 that there was no apparent pathological change in the organs of mice in the high-dose group and the low-dose group, which means that **L26** is low in toxic and safe *in vivo*.

2.2.7. *Preliminary evaluation of the pharmacokinetic (PK) characteristics of L26 in rats*

Given the favorable anti-inflammatory activity of **L26** *in vitro* and *in vivo*, we selected **L26** for preliminary pharmacokinetic evaluation in adult male SD rats. Fig. 10 showed the plasma concentration-time profile of **L26**. Next, we calculated the pharmacokinetic parameters using the Drug and Statistics (DAS) software 3.0 and a non-compartmental model to fit. As illustrated in Table 2, the active compound **L26** reached the maximum plasma concentration at T = 3.500 h with a half-life of 4.246 h. The above results indicated that **L26** was worth of further investigation for its anti-inflammatory effects.

3. Conclusions

In the present study, a series of *O*-benzyl CIN derivatives were designed and synthesized with CIN as the lead compound. The anti-inflammatory activity of the compounds was evaluated by measuring their effect on inhibiting ALP activity in Hek-blue-TLR4 cells. The promising compound **L26** was obtained and was found to suppress the expression of IL-6 and TNF-α in RAW 264.7 cells in a concentration-dependent manner. Further SAR analysis of compounds revealed that the benzimidazole ring significantly contributed to its anti-inflammatory activity. Results from ELISA and immunoprecipitation experiments indicated that **L26** targeted on MD-2 protein and competed with LPS to bind to MD-2 to inhibit inflammation, which was further confirmed by molecular docking analysis. In the mouse model of ALI,

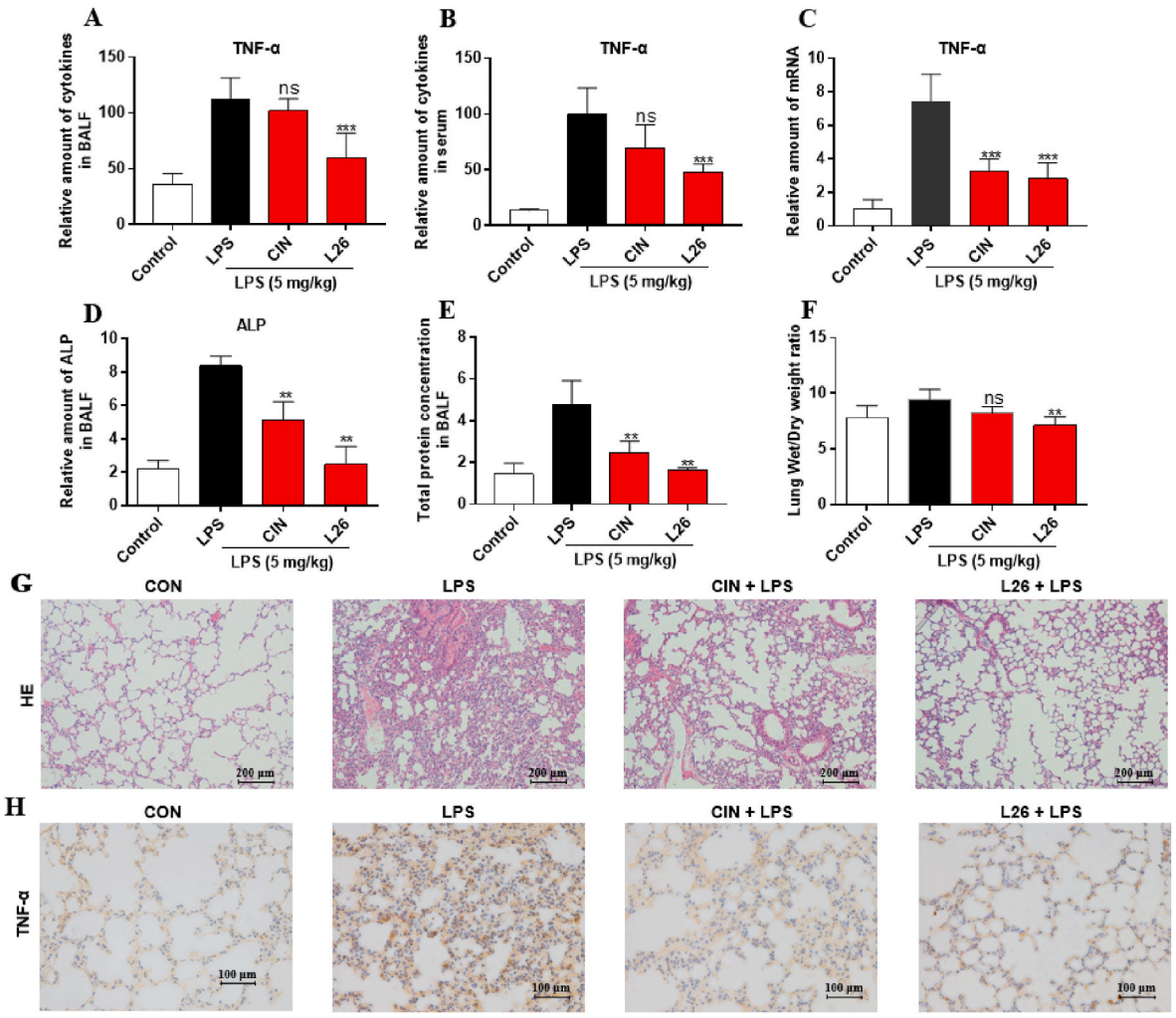

Fig. 6. Pre-treatment of mice with **L26** suppresses LPS-induced acute lung injury. C57BL/6 mice were orally administered with **L26** (5 mg/kg) or CIN (5 mg/kg) three times, followed by tracheal injection of LPS (5 mg/kg). Mice were sacrificed to obtain the lung samples after 6 h. (A, B) ELISA results for the detection of TNF-α in BALF and serum. (C) Real-time q-RTPCR assay results showing the expression level of TNF-α mRNA. (D) ELISA results for the detection of ALP in BALF. (E) Total protein concentration in BALF. (G) Representative H&E staining images of the lung (original magnification × 10). (H) Representative images of immunohistochemical staining for TNF-α in the lung tissues (original magnification × 20). Data were reported as mean ± SEM. *P < 0.05, **P < 0.01, ***P < 0.001 compared with the LPS group.

L26 alleviated tissue damage by inhibiting the NF-κB signaling pathway, resulting in the suppression of inflammation associated with ALI. Acute toxicity studies showed that **L26** did not cause adverse drug reactions and no obvious pathological damage to major organs in mice. It also exhibited excellent pharmacokinetic parameters in SD rats, with a half-life $T_{1/2} = 4.246$ h. In general, **L26** showed favorable anti-inflammatory activity *in vitro* and *in vivo* and could serve as a potential therapeutic agent for ALI treatment.

4. Experimental

4.1. General chemistry methods

Unless otherwise stated, all reagents and solvents used in the experiments were purchased from commercial vendors and used without further purification. TLC analysis was performed on silica gel plates, and the reactions were visualized under the UV light (254 nm). All melting points were measured using the Fisher-Johns melting point apparatus and were uncorrected. Flash column chromatography was performed with silica gel grade 60 (E. Merck, 70–230 mesh). All ^{1}H and ^{13}C NMR spectra reported as parts per million (ppm) were recorded on the Bruker 400 NMR spectrometers with tetramethylsilane (TMS; $\delta = 0$) as the internal standard. Data for the chemical shifts were reported as follows: chemical shift (δ ppm), multiplicity (s = singlet, d = doublet, t = triplet, q = quartet, dd = doublet of doublets, m = multiplet), coupling constants (Hz), and integration. The substrate and products were recorded on ESI quadrupole mass spectrometers (Agilent 1290 Infinity II^{+} 6135MS). The purity of some compounds was detected by HPLC (USA Agilent 1100).

4.2. General procedure for the preparation of intermediates ***1a-1j***

The *p*-hydroxybenzaldehyde (4.880 g, 40 mmol), trimethyl benzyl bromide (9.516 g, 52 mmol) and K_2CO_3 powder (11.040 g, 80 mmol) were suspended in anhydrous acetonitrile (20 mL). The reaction mixture was first flushed with nitrogen gas to establish an oxygen-free environment and then it was heated and stirred within an oil bath (bath temperature, 80 °C) for 8 h. The solution was removed by vacuum distillation to obtain a brown oily mixture. After completion, the mixture was washed with 120 mL of saturated aqueous NaCl twice and extracted three times with equal volumes of ethyl acetate. The upper organic phase was separated, collected, and dried over $MgSO_4$. After filtration, the solvent was removed by reduced pressure distillation, and 4-((3-methylbenzyl)oxy)benzaldehyde (**1a**, yield 89%) was separated by

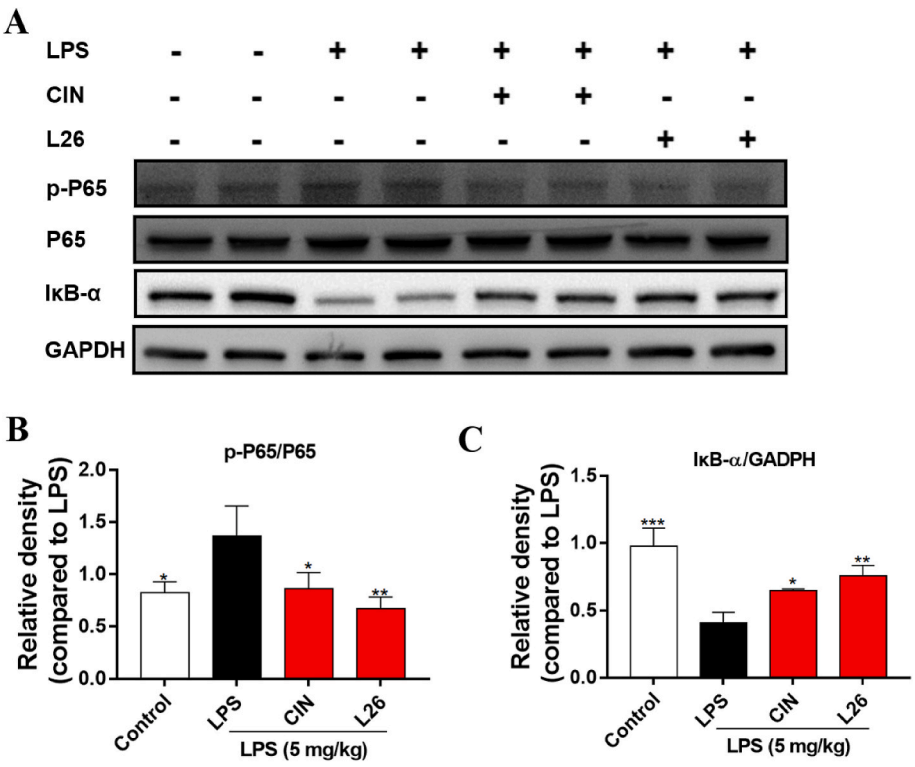

Fig. 7. L26 inhibited the NF-κB signaling pathway in the lung tissues. (A) The lung tissues were lysed with RIPA lysis buffer containing PMSF and the protein concentrations in the samples were analyzed using the Bradford colorimetric method. Antibodies against p65, phospho-p65, and its downstream targets IB- were utilized in Western blot, with GAPDH served as a reference. (B, C) Densitometric quantification of p-P65 and Iκ B-α (*P < 0.05, **P < 0.01, ***P < 0.001 compared with the LPS group).

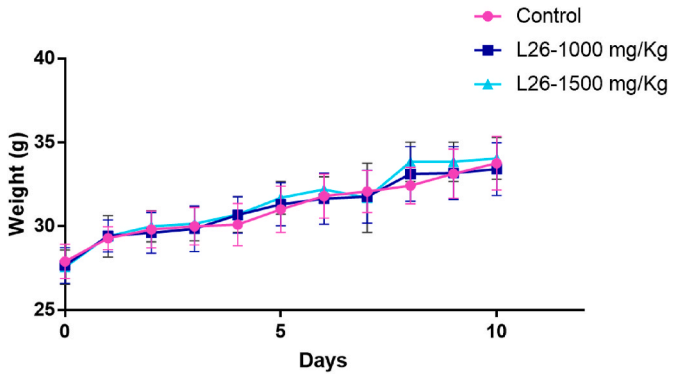

Fig. 8. Body weight of all mice in three groups (g)-time (day). Weight data expressed as standard error of the mean (SEM) of body weight.

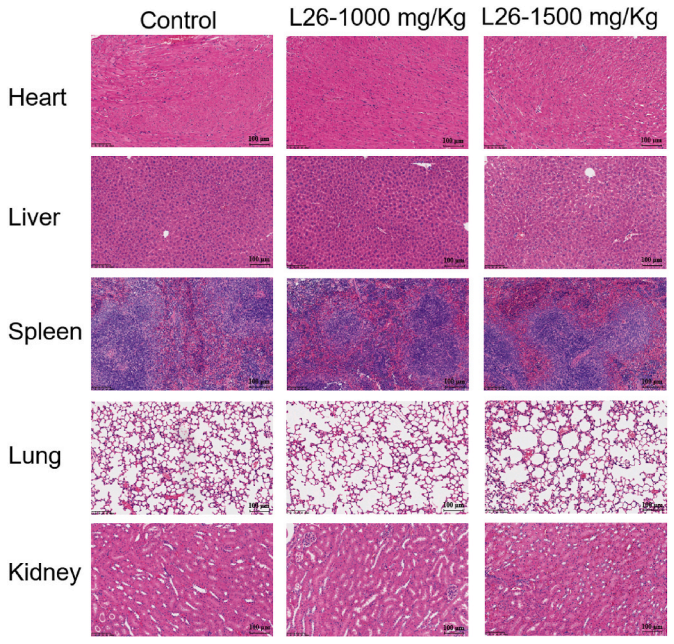

Fig. 9. Histological H&E staining of important organs (heart, liver, spleen, lung and kidney) after 10 days (original magnification × 20).

column chromatography in the mobile phase of petroleum ether: ethyl acetate = 4 : 1 (v/v). The remaining intermediates **1b**-**1j** were obtained through this scheme. The ^{1}H NMR of **1a** have been give in this paper, and the ^{1}H NMR of the remaining **1b**-**1j** can be found in Refs. [47–55].

4.3. General procedure for the preparation of intermediates *2a-2j*

4-((3-methylbenzyl)oxy)benzaldehyde (**1a**, 7.273 g, 32 mmol) and malonic acid (6.656 g, 64 mmol) were added to the reaction flask containing 5 mL pyridine solvent, then piperidine (0.340 g, 4 mmol) was added to the reaction system to catalyze the reaction. Subsequently, the reaction was allowed to stir constantly, and the solution was allowed to get uniformly heated for 4 h before the reaction completion was monitored by TLC. The reaction mixture was diluted with 0.1 M HCl, and the product was extracted into dichloromethane (50 mL × 3), dried over anhydrous magnesium sulfate, and filtered. The dichloromethane was removed under reduced pressure, and the target products were purified by silica gel column chromatography using chloroform: methanol (95 : 5) as the mobile phase. Finally, a solid white powder (*E*)-3-(4-((3-methylbenzyl)oxy)phenyl)acrylic acid (**2a**, yield 64%) was obtained. The remaining intermediates **2b-2j** were obtained via this scheme. The ^{1}H NMR of **2a, 2d, 2f, 2h, 2i** and **2j** have been given in this paper, and the ^{1}H NMR of the **2b**, **2c**, **2e** and **2g** can be found in Refs. [56–58].

4.4. General procedure for the preparation of compounds *L1-L10*

(*E*)-3-(4-((3-methylbenzyl)oxy)phenyl)acrylic acid (**2a**, 0.268 g, 1

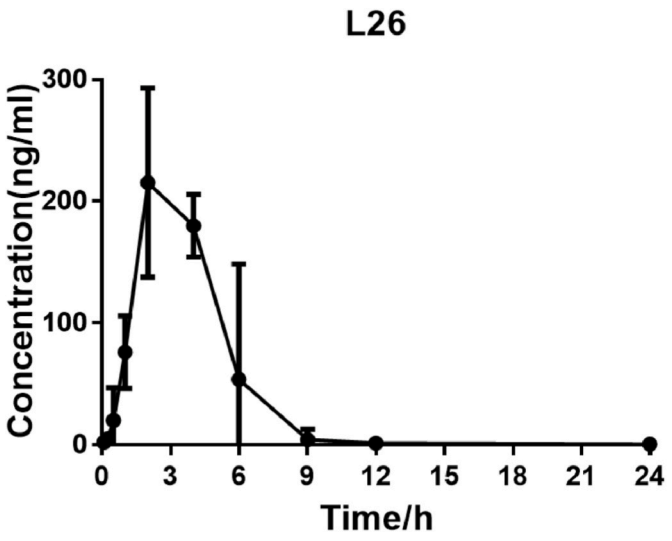

Fig. 10. Mean plasma concentration-time profiles of **L26** in rat. SD rats were treated with **L26** (10 mg/kg) through oral administration and blood samples were collected at 5 min, 15 min, 30 min, 1 h, 2 h, 4 h, 6 h, 9 h, 12 h, and 24 h.

Table 2
Pharmacokinetic parameters for compound **L26** in SD rats.

Parameters	L26
$AUC_{(0\text{-}t)}$ (μg/L*h)	461.986 ± 326.879
$AUC_{(0\text{-}\infty)}$ (μg/L*h)	464.692 ± 328.090
$T_{1/2}$ (h)	4.246 ± 3.258
T_{max} (h)	3.500 ± 2.168
C_{max} (μg/L)	163.288 ± 100.662

Data were mean concentrations in rat plasma (n = 6).

mmol) was dissolved in 5 mL ultra-dry dichloromethane, and then triethylamine (276.710 μL, 2 mmol) was slowly added to dissolve it. TBTU (0.385 g, 1.2 mmol) was selected as the condensation agent. Finally, 2-aminoimidazole (0.150 g, 1.5 mmol) was added to the solution, mixed and stirred at room temperature for 6 h. The obtained mixture was poured into saturated salt water, and 50 mL dichloromethane solution was added for extraction. Then the organic phase was dried on $MgSO_4$, and the solvent was evaporated. The crude product was subjected to purification by silica gel column chromatography, using dichloromethane/MeOH (85/15, v/v) as the mobile phase to generate (*E*)-3-(4-((3-methylbenzyl)oxy)phenyl)-*N*-(thiazol-2-yl)acrylamide (**L1**, yield 65%). Substituting **2b-2j** with **2a** as the reaction substrate, the corresponding compound **L2-L10** was obtained by the same method described in **L1**.

*4.5. General procedure for the preparation of compounds **L11-L27***

The corresponding compounds **L11-L27** were obtained by replacing 2-aminothiazole with 2-aminobenzothiazole or 2-aminobenzimidazole as the reaction substrate, and its reagent and reaction solvent were consistent with the method described for **L1**.

*4.5.1. 4-((3-methylbenzyl)oxy)benzaldehyde **(1a)***

White oil, yield: 89%. ^{1}H NMR (400 MHz, $CDCl_3$) δ 9.93 (s, 1H), 7.88 (d, J = 8.7 Hz, 2H), 7.33 (t, J = 7.5 Hz, 1H), 7.30-7.25 (m, 2H), 7.21 (d, J = 7.4 Hz, 1H), 7.12 (d, J = 8.7 Hz, 2H), 5.15 (s, 2H), 2.42 (s, 3H).

*4.5.2. (E)-3-(4-((3-methylbenzyl)oxy)phenyl)acrylic acid **(2a)***

White solid, yield: 64%. ^{1}H NMR (400 MHz, DMSO-d_6) δ 12.25 (s, 1H), 7.65 (d, J = 8.7 Hz, 2H), 7.55 (d, J = 16.0 Hz, 1H), 7.28 (p, J = 7.4 Hz, 3H), 7.16 (d, J = 7.1 Hz, 1H), 7.05 (d, J = 8.7 Hz, 2H), 6.39 (d, J = 16.0 Hz, 1H), 5.13 (s, 2H), 2.34 (s, 3H).

*4.5.3. (E)-3-(4-((3-fluorobenzyl)oxy)phenyl)acrylic acid **(2d)***

White solid, yield: 78%. ^{1}H NMR (400 MHz, DMSO-d_6) δ 12.24 (s, 1H), 7.66 (d, J = 8.3 Hz, 2H), 7.56 (d, J = 16.0 Hz, 1H), 7.46 (dd, J = 14.2, 7.4 Hz, 1H), 7.31 (d, J = 7.5 Hz, 2H), 7.18 (t, J = 8.4 Hz, 1H), 7.07 (d, J = 8.3 Hz, 2H), 6.40 (d, J = 15.9 Hz, 1H), 5.20 (s, 2H).

*4.5.4. (E)-3-(4-((3-methoxybenzyl)oxy)phenyl)acrylic acid **(2f)***

White solid, yield: 89%. ^{1}H NMR (400 MHz, DMSO-d_6) δ 12.24 (s, 1H), 7.65 (d, J = 8.7 Hz, 2H), 7.55 (d, J = 16.0 Hz, 1H), 7.40 (d, J = 8.6 Hz, 2H), 7.04 (d, J = 8.7 Hz, 2H), 6.96 (d, J = 8.6 Hz, 2H), 6.39 (d, J = 16.0 Hz, 1H), 5.08 (s, 2H), 3.77 (s, 3H).

*4.5.5. (E)-3-(4-((2,6-dichlorobenzyl)oxy)phenyl)acrylic acid **(2h)***

White solid, yield: 88%. ^{1}H NMR (400 MHz, DMSO-d_6) δ 7.64 (d, J = 8.7 Hz, 2H), 7.54 (d, J = 15.5 Hz, 2H), 7.41 (d, J = 3.4 Hz, 2H), 7.05 (d, J = 8.7 Hz, 2H), 6.39 (d, J = 16.0 Hz, 1H), 5.18 (s, 2H).

*4.5.6. (E)-3-(4-((3-chlorobenzyl)oxy)phenyl)acrylic acid **(2i)***

White solid, yield: 72%. ^{1}H NMR (400 MHz, DMSO-d_6) δ 12.29 (s, 1H), 7.67 (d, J = 8.7 Hz, 2H), 7.56 (d, J = 15.6 Hz, 2H), 7.47-7.41 (m, 3H), 7.07 (d, J = 8.7 Hz, 2H), 6.41 (d, J = 16.0 Hz, 1H), 5.20 (s, 2H).

*4.5.7. (E)-3-(4-(naphthalen-2-ylmethoxy)phenyl)acrylic acid **(2j)***

White solid, yield: 61%. ^{1}H NMR (400 MHz, DMSO-d_6) δ 12.23 (s, 1H), 8.02 (s, 1H), 7.96 (t, J = 8.6 Hz, 3H), 7.67 (d, J = 8.7 Hz, 2H), 7.61 (d, J = 8.4 Hz, 1H), 7.59-7.53 (m, 3H), 7.12 (d, J = 8.7 Hz, 2H), 6.40 (d, J = 16.0 Hz, 1H), 5.36 (s, 2H).

*4.5.8. (E)-3-(4-((3-methylbenzyl)oxy)phenyl)-N-(thiazol-2-yl)acrylamide **(L1)***

White powder, yield: 65%, m.p.: 204.7–206.1 °C. ^{1}H NMR (400 MHz, DMSO-d_6) δ 12.28 (s, 1H), 7.69 (d, J = 15.7 Hz, 1H), 7.60 (d, J = 8.6 Hz, 2H), 7.53 (d, J = 3.5 Hz, 1H), 7.29 (t, J = 6.6 Hz, 3H), 7.25 (d, J = 3.4 Hz, 1H), 7.17 (d, J = 7.2 Hz, 1H), 7.12 (d, J = 8.6 Hz, 2H), 6.80 (d, J = 15.8 Hz, 1H), 5.14 (s, 2H), 2.34 (s, 3H). LC-MS *m/z*: 373.1 [M + Na] $^+$. HPLC: t_R 3.28min, purity 97.87%.

*4.5.9. (E)-3-(4-((4-methylbenzyl)oxy)phenyl)-N-(thiazol-2-yl)acrylamide **(L2)***

White powder, yield: 55%, m.p.: 250.6–251.9 °C. ^{1}H NMR (400 MHz, $CDCl_3$, DMSO-d_6) δ 12.26 (s, 1H), 7.67 (d, J = 15.8 Hz, 1H), 7.57 (d, J = 8.7 Hz, 2H), 7.50 (d, J = 3.5 Hz, 1H), 7.34 (d, J = 7.9 Hz, 2H), 7.23 (d, J = 3.5 Hz, 1H), 7.20 (d, J = 7.8 Hz, 2H), 7.08 (d, J = 8.7 Hz, 2H), 6.77 (d, J = 15.8 Hz, 1H), 5.11 (s, 2H), 2.30 (s, 3H). ^{13}C NMR (100 MHz, DMSO) δ 163.89, 160.51, 158.78, 142.33, 138.03, 137.61, 133.82, 129.93 (2C), 129.34 (2C), 127.99 (2C), 127.52, 117.48, 115.55 (2C), 113.50, 69.85, 21.28. LC-MS *m/z*: 373.0 [M + Na] $^+$.

*4.5.10. (E)-3-(4-((4-isopropylbenzyl)oxy)phenyl)-N-(thiazol-2-yl) acrylamide **(L3)***

White powder, yield: 55%, m.p.: 219.2–221.0 °C. ^{1}H NMR (400 MHz, DMSO-d_6) δ 12.26 (s, 1H), 7.67 (d, J = 15.8 Hz, 1H), 7.58 (d, J = 8.6 Hz, 2H), 7.50 (d, J = 3.5 Hz, 1H), 7.37 (d, J = 8.0 Hz, 2H), 7.25 (dd, J = 12.0, 5.8 Hz, 3H), 7.09 (d, J = 8.6 Hz, 2H), 6.77 (d, J = 15.8 Hz, 1H), 5.11 (s, 2H), 2.89 (dt, J = 13.7, 6.9 Hz, 1H), 1.20 (d, J = 6.9 Hz, 6H). ^{13}C NMR (100 MHz, CD_3OD, $CDCl_3$, DMSO-d_6) δ 164.04, 160.62, 158.68, 148.72, 142.72, 137.77, 134.02, 129.87 (2C), 127.84 (2C), 127.40, 126.56 (2C), 116.85, 115.28 (2C), 113.35, 69.82, 33.74, 23.85 (2C). LC-MS *m/z*: 401.1 [M + Na] $^+$.

*4.5.11. (E)-3-(4-((3-fluorobenzyl)oxy)phenyl)-N-(thiazol-2-yl) acrylamide **(L4)***

White powder, yield: 54%, m.p.: 246.0–248.2 °C. ^{1}H NMR (400 MHz, DMSO-d_6) δ 12.26 (s, 1H), 7.67 (d, J = 15.7 Hz, 1H), 7.59 (d, J = 8.7 Hz,

2H), 7.50 (d, J = 3.5 Hz, 1H), 7.45 (dd, J = 14.0, 8.0 Hz, 1H), 7.30 (d, J = 8.3 Hz, 2H), 7.23 (d, J = 3.5 Hz, 1H), 7.17 (t, J = 8.1 Hz, 1H), 7.11 (d, J = 8.7 Hz, 2H), 6.78 (d, J = 15.8 Hz, 1H), 5.20 (s, 2H). LC-MS *m/z*: 377.1 [M + Na] $^+$. HPLC: t_R 3.06 min, purity 94.58%.

4.5.12. (E)-3-(4-((4-fluorobenzyl)oxy)phenyl)-N-(thiazol-2-yl) acrylamide (L5)

White powder, yield: 67%, m.p.: 275.7–277.1 °C. ^{1}H NMR (400 MHz, DMSO-d_6) δ 12.27 (s, 1H), 7.67 (d, J = 15.8 Hz, 1H), 7.59 (d, J = 8.7 Hz, 2H), 7.52 (dd, J = 8.4, 4.7 Hz, 3H), 7.23 (dd, J = 10.5, 7.2 Hz, 3H), 7.10 (d, J = 8.7 Hz, 2H), 6.78 (d, J = 15.8 Hz, 1H), 5.15 (s, 2H). LC-MS *m/z*: 377.1 [M + Na] $^+$.

4.5.13. (E)-3-(4-((3-methoxybenzyl)oxy)phenyl)-N-(thiazol-2-yl) acrylamide (L6)

White powder, yield: 37%, m.p.: 193.0–195.2 °C. ^{1}H NMR (400 MHz, DMSO-d_6) δ 12.26 (s, 1H), 7.67 (d, J = 15.8 Hz, 1H), 7.58 (d, J = 8.7 Hz, 2H), 7.50 (d, J = 3.5 Hz, 1H), 7.31 (t, J = 8.1 Hz, 1H), 7.23 (d, J = 3.5 Hz, 1H), 7.09 (d, J = 8.7 Hz, 2H), 7.05-6.97 (m, 2H), 6.90 (dd, J = 8.1, 2.1 Hz, 1H), 6.78 (d, J = 15.8 Hz, 1H), 5.14 (s, 2H), 3.76 (s, 3H). ^{13}C NMR (100 MHz, DMSO-d_6) δ 163.91, 160.55, 159.85, 158.69, 142.49, 138.77, 138.36, 130.21 (2C), 130.10, 127.60, 120.27, 117.58, 115.89 (2C), 114.18, 113.84, 113.71, 69.72, 55.55. LC-MS *m/z*: 389.1 [M + Na] $^+$. HPLC: t_R 3.10 min, purity 99.7%.

4.5.14. (E)-3-(4-((4-methoxybenzyl)oxy)phenyl)-N-(thiazol-2-yl) acrylamide (L7)

White powder, yield: 59%, m.p.: 233.3–234.2 °C. ^{1}H NMR (400 MHz, DMSO-d_6) δ 12.26 (s, 1H), 7.67 (d, J = 15.7 Hz, 1H), 7.57 (d, J = 8.4 Hz, 2H), 7.51 (d, J = 3.3 Hz, 1H), 7.39 (d, J = 8.3 Hz, 2H), 7.23 (d, J = 3.3 Hz, 1H), 7.08 (d, J = 8.4 Hz, 2H), 6.95 (d, J = 8.3 Hz, 2H), 6.77 (d, J = 15.8 Hz, 1H), 5.07 (s, 2H), 3.75 (s, 3H). LC-MS *m/z*: 389.1 [M + Na] $^+$. HPLC: t_R 3.09 min, purity 97.42%.

4.5.15. (E)-3-(4-((2,6-dichlorobenzyl)oxy)phenyl)-N-(thiazol-2-yl) acrylamide (L8)

White powder, yield: 78%, m.p.: 246.7–247.8 °C. ^{1}H NMR (400 MHz, DMSO-d_6) δ 12.27 (s, 1H), 7.67 (d, J = 15.8 Hz, 1H), 7.59 (d, J = 8.4 Hz, 2H), 7.55-7.49 (m, 2H), 7.43 (s, 2H), 7.23 (d, J = 3.2 Hz, 1H), 7.11 (d, J = 8.4 Hz, 2H), 6.78 (d, J = 15.7 Hz, 1H), 5.19 (s, 2H). ^{13}C NMR (100 MHz, DMSO-d_6) δ 163.89, 160.31, 158.68, 142.44, 139.79, 138.36, 133.64, 130.91, 130.23 (2C), 128.36, 127.87, 127.79, 126.74, 117.71, 115.89 (2C), 114.19, 68.91. LC-MS *m/z*: 426.2 [M + Na] $^+$. HPLC: t_R 3.25 min, purity 96.72%.

4.5.16. (E)-3-(4-((3-chlorobenzyl)oxy)phenyl)-N-(thiazol-2-yl) acrylamide (L9)

White powder, yield: 62%, m.p.: 244.1–245.6 °C. ^{1}H NMR (400 MHz, DMSO-d_6) δ 12.29 (s, 1H), 7.69 (d, J = 15.8 Hz, 1H), 7.61 (d, J = 8.6 Hz, 2H), 7.55 (s, 1H), 7.53 (d, J = 3.5 Hz, 1H), 7.44 (d, J = 3.3 Hz, 3H), 7.26 (d, J = 3.5 Hz, 1H), 7.13 (d, J = 8.6 Hz, 2H), 6.80 (d, J = 15.8 Hz, 1H), 5.21 (s, 2H). ^{13}C NMR (100 MHz, $CDCl_3$, DMSO) δ 163.84, 160.22, 158.74, 142.29, 139.56, 138.14, 133.82, 130.59, 130.07 (2C), 128.21, 127.81, 127.68, 126.35, 117.72, 115.70 (2C), 113.78, 68.95. LC-MS *m/z*: 393.0 [M + Na] $^+$. HPLC: t_R 3.25 min, purity 97.11%.

4.5.17. (E)-3-(4-(naphthalen-2-ylmethoxy)phenyl)-N-(thiazol-2-yl) acrylamide (L10)

White powder, yield: 68%, m.p.: 266.1–267.2 °C. ^{1}H NMR (400 MHz, DMSO-d_6) δ 12.25 (s, 1H), 8.00 (s, 1H), 7.94 (dd, J = 11.7, 5.8 Hz, 3H), 7.67 (d, J = 15.7 Hz, 1H), 7.59 (d, J = 8.5 Hz, 3H), 7.53 (dd, J = 5.7, 3.5 Hz, 2H), 7.50 (d, J = 3.5 Hz, 1H), 7.23 (d, J = 3.5 Hz, 1H), 7.15 (d, J = 8.6 Hz, 2H), 6.78 (d, J = 15.8 Hz, 1H), 5.34 (s, 2H). LC-MS *m/z*: 409.1 [M + Na] $^+$.

4.5.18. (E)-N-(benzo[d]thiazol-2-yl)-3-(4-((3-methylbenzyl)oxy)phenyl) acrylamide (L11)

White powder, yield: 64%, m.p.: 237.1–238.5 °C. ^{1}H NMR (400 MHz, DMSO-d_6) δ 12.52 (s, 1H), 7.99 (d, J = 6.2 Hz, 1H), 7.76 (d, J = 8.4 Hz, 2H), 7.62 (d, J = 6.1 Hz, 2H), 7.44 (s, 1H), 7.27 (s, 4H), 7.13 (d, J = 11.1 Hz, 3H), 6.82 (d, J = 15.5 Hz, 1H), 5.12 (s, 2H), 2.32 (s, 3H). LC-MS *m/z*: 239.2 [M/2 + K] $^+$.

4.5.19. (E)-N-(benzo[d]thiazol-2-yl)-3-(4-((4-methylbenzyl)oxy)phenyl) acrylamide (L12)

White powder, yield: 32%, m.p.: 248.3–249.2 °C. ^{1}H NMR (400 MHz, DMSO-d_6) δ 12.51 (s, 1H), 7.99 (d, J = 7.6 Hz, 1H), 7.85-7.69 (m, 2H), 7.61 (d, J = 7.9 Hz, 2H), 7.44 (t, J = 7.3 Hz, 1H), 7.32 (dd, J = 17.2, 7.5 Hz, 3H), 7.20 (d, J = 7.2 Hz, 2H), 7.09 (d, J = 7.9 Hz, 2H), 6.81 (d, J = 15.7 Hz, 1H), 5.12 (s, 2H), 2.30 (s, 3H). ^{13}C NMR (100 MHz, $CDCl_3$, DMSO-d_6) δ 164.89, 160.64, 158.68, 149.16, 143.26, 137.77, 133.48, 132.30, 129.98 (2C), 129.30 (2C), 127.74 (2C), 127.38, 125.94, 123.46, 121.27, 120.76, 117.05, 115.33 (2C), 69.95, 21.24. LC-MS *m/z*: 423.1 [M + Na] $^+$.

4.5.20. (E)-N-(benzo[d]thiazol-2-yl)-3-(4-((4-isopropylbenzyl)oxy) phenyl)acrylamide (L13)

White powder, yield: 69%, m.p.: 165.7–167.7 °C. ^{1}H NMR (400 MHz, $CDCl_3$) δ 8.57 (d, J = 8.4 Hz, 1H), 8.12-8.04 (m, 2H), 7.83 (t, J = 7.8 Hz, 1H), 7.69 (d, J = 8.6 Hz, 2H), 7.60 (dd, J = 15.6, 10.2 Hz, 2H), 7.41 (d, J = 7.9 Hz, 2H), 7.32 (s, 2H), 7.07 (d, J = 8.6 Hz, 2H), 5.13 (s, 2H), 3.16-2.78 (m, 1H), 1.30 (d, J = 6.9 Hz, 6H). ^{13}C NMR (100 MHz, $CDCl_3$) δ 162.07, 161.92, 149.65, 149.16, 149.04, 133.62, 133.51, 132.96, 132.86, 131.06 (2C), 127.78 (2C), 126.91, 126.83 (2C), 126.76, 116.54, 115.50 (2C), 114.60, 112.15, 70.21, 33.95, 24.02 (2C).

4.5.21. (E)-N-(benzo[d]thiazol-2-yl)-3-(4-((3-fluorobenzyl)oxy)phenyl) acrylamide (L14)

White powder, yield: 59%, m.p.: 181.4–182.0 °C. ^{1}H NMR (400 MHz, DMSO-d_6) δ 8.46 (d, J = 8.4 Hz, 1H), 8.07 (dd, J = 11.8, 8.8 Hz, 2H), 7.95 (d, J = 7.5 Hz, 1H), 7.93-7.86 (m, 2H), 7.70 (t, J = 7.8 Hz, 1H), 7.48 (dd, J = 18.3, 11.8 Hz, 2H), 7.34 (d, J = 8.5 Hz, 2H), 7.18 (dd, J = 20.8, 8.3 Hz, 3H), 5.26 (s, 2H). LC-MS *m/z*: 443.1 [M + K] $^+$.

4.5.22. (E)-N-(benzo[d]thiazol-2-yl)-3-(4-((4-fluorobenzyl)oxy)phenyl) acrylamide (L15)

White powder, yield: 64%, m.p.: 164.2–166.2 °C. ^{1}H NMR (400 MHz, DMSO-d_6) δ 8.45 (d, J = 8.4 Hz, 1H), 8.08-7.99 (m, 2H), 7.90 (t, J = 7.8 Hz, 1H), 7.83 (d, J = 8.5 Hz, 2H), 7.66 (t, J = 7.7 Hz, 1H), 7.49 (dd, J = 15.5, 11.9 Hz, 3H), 7.19 (t, J = 8.6 Hz, 2H), 7.11 (d, J = 8.4 Hz, 2H), 5.17 (s, 2H). LC-MS *m/z*: 427.7 [M + Na] $^+$. HPLC: t_R 3.30 min, purity 94.58%.

4.5.23. (E)-N-(benzo[d]thiazol-2-yl)-3-(4-((3-methoxybenzyl)oxy) phenyl)acrylamide (L16)

White powder, yield: 46%, m.p.: 172.4–174.4 °C. ^{1}H NMR (400 MHz, DMSO-d_6) δ 8.44 (d, J = 8.4 Hz, 1H), 8.05 (dd, J = 11.9, 9.8 Hz, 2H), 7.92 (t, J = 7.8 Hz, 1H), 7.87 (d, J = 8.7 Hz, 2H), 7.68 (t, J = 7.8 Hz, 1H), 7.48 (d, J = 15.8 Hz, 1H), 7.32 (t, J = 8.1 Hz, 1H), 7.13 (d, J = 8.7 Hz, 2H), 7.03 (d, J = 6.6 Hz, 2H), 6.91 (dd, J = 8.1, 1.8 Hz, 1H), 5.18 (s, 2H), 3.76 (s, 3H). ^{13}C NMR (100 MHz, $CDCl_3$) δ 162.05, 161.74, 159.94, 148.98 (2C), 137.82, 132.96, 132.87 (2C), 131.06 (2C), 129.81, 127.04, 126.77, 119.62, 116.53, 115.53 (3C), 113.71, 112.96, 112.26, 70.08, 55.31. HPLC: t_R 3.46 min, purity 95.33%.

4.5.24. (E)-N-(benzo[d]thiazol-2-yl)-3-(4-((4-methoxybenzyl)oxy) phenyl)acrylamide (L17)

White powder, yield: 37%, m.p.: 231.3–233.3 °C. ^{1}H NMR (400 MHz, $CDCl_3$) δ 8.53 (d, J = 8.4 Hz, 1H), 8.14-7.98 (m, 2H), 7.79 (t, J = 7.8 Hz, 1H), 7.66 (d, J = 8.6 Hz, 2H), 7.56 (dd, J = 15.6, 10.6 Hz, 2H), 7.37 (d, J = 8.5 Hz, 2H), 7.03 (d, J = 8.6 Hz, 2H), 6.93 (d, J = 8.5 Hz, 2H), 5.06 (s,

2H), 3.83 (s, 3H). ^{13}C NMR (100 MHz, $CDCl_3$) δ 162.08, 161.89, 159.69, 149.05 (2C), 132.97, 132.87, 131.05 (2C), 129.31 (2C), 128.21, 126.91, 126.76, 116.53, 115.52 (3C), 114.15 (2C), 112.16 (2C), 70.05, 55.36. HPLC: t_R 3.34 min, purity 95.11%.

4.5.25. (E)-N-(benzo[d]thiazol-2-yl)-3-(4-((2,6-dichlorobenzyl)oxy) phenyl)acrylamide (**L18**)

White powder, yield: 76%, m.p.: 272.3–273.6 °C. ^{1}H NMR (400 MHz, DMSO-d_6) δ 12.52 (s, 1H), 8.00 (s, 1H), 7.76 (s, 2H), 7.63 (s, 2H), 7.54 (s, 1H), 7.43 (s, 3H), 7.31 (s, 1H), 7.13 (s, 2H), 6.82 (d, J = 14.9 Hz, 1H), 5.20 (s, 2H). LC-MS *m/z*: 304.3 [M/2 + K*2] $^+$.

4.5.26. (E)-N-(benzo[d]thiazol-2-yl)-3-(4-((3-chlorobenzyl)oxy)phenyl) acrylamide (**L19**)

White powder, yield: 59%, m.p.: 185.8–187.5 °C. ^{1}H NMR (400 MHz, $CDCl_3$) δ 8.53 (d, J = 8.4 Hz, 1H), 8.08-7.98 (m, 2H), 7.79 (t, J = 7.8 Hz, 1H), 7.66 (d, J = 8.6 Hz, 2H), 7.57 (dd, J = 15.6, 8.1 Hz, 2H), 7.45 (s, 1H), 7.33 (s, 3H), 7.03 (d, J = 8.6 Hz, 2H), 5.11 (s, 2H). LC-MS *m/z*: 249.1 [M/2 + K] $^+$. HPLC: t_R 5.49 min, purity 95.84%.

4.5.27. (E)-N-(benzo[d]thiazol-2-yl)-3-(4-(naphthalen-2-ylmethoxy) phenyl)acrylamide (**L20**)

White powder, 64% yield, m.p.: 201.3–203.1 °C. ^{1}H NMR (400 MHz, DMSO-d_6) δ 8.18 (d, J = 11.6 Hz, 1H), 8.04 (s, 1H), 7.96 (t, J = 7.8 Hz, 5H), 7.66 (dd, J = 21.5, 9.1 Hz, 3H), 7.56 (s, 4H), 7.23 (d, J = 8.2 Hz, 2H), 7.15-7.06 (m, 1H), 5.42 (s, 2H). LC-MS *m/z*: 437.2 [M + H] $^+$.

4.5.28. (E)-N-(1H-benzo[d]imidazole-2-yl)-3-(4-((4-methylbenzyl)oxy) phenyl)acrylamide (**L21**)

Orange powder, yield: 64%, m.p.: 105.2–107.1 °C. ^{1}H NMR (400 MHz, DMSO-d_6) δ 7.91 (d, J = 15.6 Hz, 1H), 7.84 (d, J = 8.7 Hz, 2H), 7.46 (d, J = 8.0 Hz, 1H), 7.40-7.33 (m, 3H), 7.24 (dd, J = 11.0, 8.1 Hz, 4H), 7.18 (d, J = 7.4 Hz, 1H), 7.13 (d, J = 8.7 Hz, 1H), 7.04 (dd, J = 9.0, 5.5 Hz, 1H), 5.17 (s, 2H), 2.33 (s, 3H). LC-MS *m/z*: 384.1 [M + H] $^+$. HPLC: t_R 3.60 min, purity 96.50%.

4.5.29. (E)-N-(1H-benzo[d]imidazole-2-yl)-3-(4-((3-fluorobenzyl)oxy) phenyl)acrylamide (**L22**)

Orange powder, yield: 66%, m.p.: 153.5–155.4 °C. ^{1}H NMR (400 MHz, DMSO-d_6) δ 7.92 (d, J = 15.6 Hz, 1H), 7.85 (d, J = 8.7 Hz, 2H), 7.49-7.45 (m, 2H), 7.35 (dd, J = 15.2, 12.0 Hz, 3H), 7.25 (d, J = 7.4 Hz, 2H), 7.20 (d, J = 3.6 Hz, 1H), 7.16 (d, J = 8.9 Hz, 2H), 7.05 (dd, J = 14.4, 7.0 Hz, 1H), 5.25 (s, 2H). LC-MS *m/z*: 388.1 [M + H] $^+$. HPLC: t_R 3.59 min, purity 99.14%.

4.5.30. (E)-N-(1H-benzo[d]imidazole-2-yl)-3-(4-((4-fluorobenzyl)oxy) phenyl)acrylamide (**L23**)

Orange powder, yield: 72%, m.p.: 226.1–227.8 °C. ^{1}H NMR (400 MHz, DMSO-d_6) δ 7.92 (d, J = 15.6 Hz, 1H), 7.85 (d, J = 8.7 Hz, 2H), 7.55 (dd, J = 8.6, 5.7 Hz, 2H), 7.47 (d, J = 8.0 Hz, 1H), 7.37 (d, J = 15.6 Hz, 1H), 7.26 (t, J = 7.7 Hz, 4H), 7.18-7.14 (m, 2H), 7.05 (dd, J = 11.2, 4.2 Hz, 1H), 5.21 (s, 2H). ^{13}C NMR (100 MHz, $CDCl_3$, DMSO-d_6) δ 166.81, 163.55, 161.24, 154.75, 147.16, 143.82, 133.27, 133.24, 131.35 (2C), 130.78, 130.49, 130.41, 127.37, 124.36, 120.31, 117.31, 116.31, 115.87 (2C), 115.65, 113.44, 69.23. LC-MS *m/z*: 388.1 [M + H] $^+$. HPLC: t_R 3.27 min, purity 99.20%.

4.5.31. (E)-N-(1H-benzo[d]imidazole-2-yl)-3-(4-((2,6-dichlorobenzyl) oxy)phenyl)acrylamide (**L24**)

Orange powder, yield: 65%, m.p.: 165.1–166.7 °C. ^{1}H NMR (400 MHz, DMSO-d_6) δ 7.94 (d, J = 15.5 Hz, 1H), 7.88 (d, J = 8.6 Hz, 2H), 7.60 (d, J = 7.9 Hz, 2H), 7.52 (d, J = 7.3 Hz, 1H), 7.48 (d, J = 8.6 Hz, 1H), 7.39 (d, J = 15.6 Hz, 1H), 7.24 (dd, J = 14.3, 8.0 Hz, 4H), 7.17 (t, J = 7.6 Hz, 1H), 7.05 (t, J = 7.8 Hz, 1H), 5.34 (s, 2H). ^{13}C NMR (100 MHz, $CDCl_3$, DMSO-d_6) δ 166.76, 161.40, 154.77, 147.09, 143.83, 136.67 (2C), 131.86, 131.74, 131.26 (2C), 130.69, 129.08 (2C), 127.64, 124.32, 120.22, 117.39, 116.33, 115.60 (2C), 113.35, 65.53. LC-MS *m/z*: 439.1 [M + Na] $^+$. HPLC: t_R 3.89 min, purity 95.09%.

4.5.32. (E)-N-(1H-benzo[d]imidazole-2-yl)-3-(4-((3-chlorobenzyl)oxy) phenyl)acrylamide (**L25**)

Orange powder, yield: 74%, m.p.: 152.3–154.1 °C. ^{1}H NMR (400 MHz, DMSO-d_6) δ 7.89 (d, J = 15.6 Hz, 1H), 7.81 (d, J = 8.3 Hz, 2H), 7.44 (d, J = 7.8 Hz, 1H), 7.40 (d, J = 8.3 Hz, 2H), 7.33 (d, J = 15.7 Hz, 1H), 7.23 (d, J = 2.8 Hz, 2H), 7.13 (dd, J = 18.9, 7.9 Hz, 3H), 7.02 (t, J = 7.4 Hz, 1H), 6.95 (d, J = 8.2 Hz, 2H), 5.11 (s, 2H), 3.76 (s, 3H). LC-MS *m/z*: 404.1 [M + H] $^+$. HPLC: t_R 3.29 min, purity 97.02%.

4.5.33. (E)-N-(1H-benzo[d]imidazole-2-yl)-3-(4-((3-methoxybenzyl)oxy) phenyl)acrylamide (**L26**)

Orange powder, yield: 49%, m.p.: 147.2–148.9 °C. ^{1}H NMR (400 MHz, DMSO-d_6) δ 7.92 (d, J = 15.5 Hz, 1H), 7.85 (d, J = 8.7 Hz, 2H), 7.47 (d, J = 8.0 Hz, 1H), 7.40-7.31 (m, 2H), 7.26 (d, J = 8.3 Hz, 2H), 7.16 (dd, J = 15.1, 8.1 Hz, 3H), 7.05 (d, J = 6.4 Hz, 2H), 6.93 (dd, J = 8.1, 2.0 Hz, 1H), 5.20 (s, 2H), 3.78 (s, 3H). ^{13}C NMR (100 MHz, DMSO-d_6) δ 166.85, 161.31, 159.85, 154.73, 147.17, 143.80, 138.71, 131.43 (2C), 130.83, 130.13, 127.35, 124.41, 120.40, 120.26, 117.38, 116.31, 115.94 (2C), 113.85, 113.72, 113.50, 69.77, 55.56. LC-MS *m/z*: 400.1 [M + H] $^+$. HPLC: t_R 3.35 min, purity 96.73%.

4.5.34. (E)-N-(1H-benzo[d]imidazole-2-yl)-3-(4-(naphthalen-2-ylmethoxy)phenyl)acrylamide (**L27**)

Orange powder, yield: 62%, m.p.: 212.3–213.9 °C. ^{1}H NMR (400 MHz, DMSO-d_6) δ 8.01 (s, 1H), 7.95 (t, J = 9.3 Hz, 3H), 7.89-7.82 (m, 2H), 7.60 (d, J = 8.2 Hz, 1H), 7.54 (s, 2H), 7.44 (d, J = 7.8 Hz, 1H), 7.34 (d, J = 15.5 Hz, 1H), 7.23 (s, 2H), 7.16 (dd, J = 17.9, 8.1 Hz, 3H), 7.02 (t, J = 7.5 Hz, 1H), 5.38 (s, 2H). LC-MS *m/z*: 420.2 [M + H] $^+$. HPLC: t_R 3.94 min, purity 95.15%.

4.6. Cells and biological reagents

Hek-blue-TLR4 cells and Mouse RAW 264.7 macrophages were purchased from the China Center for Type Culture Collection (CCTCC, Wuhan, China). ALP kit was purchased from Solarbio (Beijing, China, G1480). LPS was purchased from Sigma-Aldrich (St Louis, MO, USA). TNF-α ELISA kits were purchased from eBioscience Inc. (San Diego, CA, USA). LPS was purchased from Sigma-Aldrich (St. Louis, MO, USA). Recombinant human MD-2 (rhMD-2) and rhTLR4 proteins were purchased from R&D (Minneapolis, MN, USA). Antibodies against MD-2, TLR4, P65, p-P65, GAPDH, and IκBα were procured from Cell Signaling Technology (Danvers, MA, USA). Briefly, Hek-blue-TLR4 cells and Mouse RAW 264.7 macrophages were cultured in DMEM supplemented with 10% FBS and penicillin/streptomycin. For the *in vivo* experiments, all compounds were dissolved in DMSO and diluted with DMEM to a final DMSO concentration of 0.1%.

4.7. In vitro anti-inflammatory effects of the compounds against Hek-blue-TLR4 cells

The anti-inflammatory effects of the compounds were assessed by evaluating their effects on the inhibition of ALP activity in Hek-blue-TLR4 cells. After pre-treatment with the compounds and LPS, the ALP activity in the supernatants of LPS-stimulated cells were determined using the Alkaline Phosphatase assay kit. Briefly, on the first day, Hek-blue-TLR4 cells were cultured in 96-well plates (2×10^4 cells per well) at 37 °C under 5% CO_2 atmosphere for 24 h in 100 μL DMEM (10% FBS and 1% penicillin/streptomycin). The cells were pre-treated with the compound or DMSO for 0.5 h, followed by treatment with LPS (0.5 μg/mL) for another 24 h. 15 μL of the sample buffer was collected and transferred from each well of the cell culture plates to a transparent 96-well plate. According to the manufacturer's instructions, the assay reagent (85 μL) was added to the 96-well plate. Using a plate reader, the

absorbance was measured at 405 nm (OD 405). Finally, we analyzed the data on the Origin 8.5 software.

4.8. MTT assay

Firstly, Hek-blue-TLR4 were seeded in 96-well plates at a density of 4000 cells/well. The cells were cultured for 12 h, and then treated with the compounds for 4 h. Then, each well was filled with 25 mL of MTT solution (0.5 mg/mL) (Sigma-Aldrich, St. Louis, MO), and the cells were incubated under 5% CO_2 atmosphere at 37 °C for 4 h. The optical density (OD; A value) was measured using a plate reader at a wavelength of 490 nm.

4.9. Competition with LPS bound on MD-2

We evaluated the ability of **L26** to compete with biotin-labeled LPS (biotin-LPS) bound to recombinant human-MD-2 (rhMD-2) using ELISA. Anti-rhMD-2 antibody was seeded in 96-well plates at 4 °C for 12 h. The 10 mM Tris-HCl of rhMD-2 (4 μg/mL) buffer was added to the pre-coated plates for 1.5 h at room temperature. The plates were washed with PBST, and biotin-labeled LPS was added to the plate with or without **L26** (1 μM). The absorbance was measured using a plate reader at a wavelength of 450 nm (OD 450) and analyzed using the Origin 8.5 software.

4.10. Western blotting and immunoprecipitation

The cells were seeded in 6-well plates (500,000 cells per well) for 12 h, followed by treatment with cinnamic or **L26** for overnight. After this, the cells were lysed with RIPA lysis buffer (RIPA; Millipore Sigma) containing PMSF (Beyotime, Code ST506), according to the manufacturer's instructions. The protein concentrations in the samples were analyzed using the Bradford colorimetric method and the samples were separated by 10% SDS-PAGE and transferred onto PVDF membranes. Then, the membranes were incubated in 3% bovine serum albumin for 1 h to block non-specific binding and were washed with Tris-buffered saline containing Tween 20 (TBST) buffer for 5 min. The antibody was diluted to 1: 2000 and incubated with the membrane at 4 °C for overnight. The membrane was rinsed thrice with TBST, then incubated with the secondary antibody in TBST-10% blocking reagent for 1 h before being rewashed in TBST (three times for 20 min). The protein bands were detected using Kodak exposure films.

For the immunoprecipitation assay, the cells were prepared and incubated at 4 °C with the anti-TLR4 antibody for 12 h. The immune complexes were precipitated with protein A + G agarose, and the precipitates were washed five times with ice cold PBS. After being boiled in the loading buffer, the samples were subjected to Western blot analysis.

4.11. Real-time quantitative PCR

The total RNA from the lung tissue was extracted according to the manufacturer's instructions for the RNeasy kit (Takara, Shiga, Japan). Both reverse transcription and quantitative PCR (qPCR) were conducted using a two-step M-MLV Platinum SYBR Green qPCR SuperMix-UDG kit (Invitrogen). qPCR analysis was performed using the Eppendorf Mastercycler eprealplex detection system (Eppendorf, Hamburg, Germany). The primers for the genes including TNF-α, and β-actin, were purchased from Invitrogen. The expression of each gene was determined and normalized against the expression of β-actin, and the primer sequences of the mouse genes were as follows (Invitrogen): TNF-α sense: 50-TGGAACTGGCAGAAGAGG-30; antisense: 50-AGACAGAAGAGCGTGGTG-30; b-actin sense: 50-TGGAATCCTGTGGCATCCATGAAAC-30; antisense: 50-TAAAACGCAGCTCAGTAACAGTCCG-30.

4.12. Animal model of ALI

Male C57BL/6 mice (n = 32) of 18–22 g were obtained from the Animal Centre of Wenzhou Medical University (Wenzhou, China, ethics number wydw 2021-0353). All the animals were housed in polycarbonate cages in a light-controlled (12 h/12 h cycle) and temperature-controlled (23–25 °C) room, and the mice were fed a standard rodent diet and had free access to water and food. All the animals in this study were handled according to the Guide for Care and Use of Laboratory Animals from the National Institutes of Health. The Animal Policy and Welfare Committee of Wenzhou Medical College approved all the animal care and experimental protocols.

L26 and cinnamic were dissolved in 0.5% sodium carboxyl methyl cellulose in water solution. The animals were randomly divided into 4 groups, with 8 mice per group. Following were the four groups: control group; LPS group; Cinnamic -5 mg/kg + LPS group; and **L26**-5 mg/kg + LPS group. Cinnamic -5 mg/kg + LPS group and **L26**-5 mg/kg + LPS group were orally administered with Cinnamic (CMC-Na) or **L26** (CMC-Na) every 12 h for 36 h. Mice in the control group were orally administered with 0.5% CMC-Na solution every 12 h for 36 h. The animals were intratracheally instilled with 5 mg/kg LPS just 12 h after the last administration, and the control groups received sham surgery. The mice were euthanized with chloral hydrate 6 h after the LPS challenge. The blood samples (750 μL) were collected from the right ventricle orbital veniplex. At the end of the experiment, BALF was obtained by rinsing the left lung with 200 μL saline solution (× 4). Following centrifugation (1000 rpm, 4 °C, 10 min), the protein concentration in the supernatant was determined using the BCA protein assay (Pierce, Rockford, IL, USA). Lung edema was assessed by determining the lung wet/dry ratio, which was calculated by dividing the wet weight of each lung by its dry weight. The middle lobe of the right lung was excised and weighed immediately (wet weight) as well as after drying at 65 °C for 48 h (dry weight), and the wet/dry weight ratio was calculated.

4.13. Histopathological examination of the lung tissues from mice

For generating paraffin-embedded tissue sections, lung tissues from the mice were harvested and fixed in 4% PFA and processed, followed by their embedding in paraffin. Paraffin blocks containing the samples were then sectioned into 5 μm thick slices, and the slices were stained with Hematoxylin and Eosin (H&E assay kit, Beyotime, Shanghai, China).

For the immunohistochemical analysis, the tissue sections were deparaffinized with dimethylbenzene and rehydrated by exposure to a graded series of ethanol solutions. This was followed by subjecting the sections to antigen retrieval by boiling for 25 min in the antigen retrieval sodium citrate buffer (pH 6). Next, the sections were incubated with the specific primary antibodies at 4 °C for 12 h followed by incubation with the secondary antibodies (1: 200; Santa Cruz, USA). The slices were detected by 3,3-diaminobenzidine (DAB) (ZSGB-Bio, Beijing, China), counterstained with hematoxylin, and visualized under the microscope (Carl Zeiss).

4.14. Determination of the concentrations of TNF-α and ALP

According to the manufacturer's instructions, ELISA was conducted to determine the concentrations of TNF-α or ALP in the animal samples (BALF, serum). The amount of TNF-α and ALP were normalized to the total protein concentration in each sample.

4.15. Acute toxicity studies

ICR mice (n = 24) of 27 g ± 1 g were obtained from the Animal Centre of Wenzhou Medical University (Wenzhou, China, ethics number wydw 2021-0353). **L26** was dissolved in CMC-Na with DMSO (<0.1%), the concentration of **L26** was 50 mg/mL. Mice were treated with **L26** at the corresponding concentrations by oral gavage. Body weight, water/food intake, behavioral statuses, were monitored and recorded daily throughout the study period. After 10 days, all mice were sacrificed

under general anesthesia after injection and their vital organs (heart, liver, lung, spleen, and kidney) were harvested. Collected vital organs were subjected to pathological analysis by HE staining.

4.16. Pharmacokinetic analysis of **L26**

Male SD rats (n = 6) of 200 g ± 20 g were obtained from the Animal Centre of Wenzhou Medical University (Wenzhou, China, ethics number wydw 2022-0013). **L26** was dissolved in CMC-Na with DMSO (<0.1%), the concentration of **L26** was 10 mg/mL. The rats received 10 mg/kg of **L26** by oral gavage. Then, the blood samples were obtained from caudal vein bleeding and transferred into tubes (1.5 mL heparin sodium) at 5 min, 15 min, 30 min, 1 h, 2 h, 4 h, 6 h, 9 h, 12 h, and 24 h. The samples were centrifuged for 5 min at 13000 rpm and 300 μL of the supernatant was transferred into a new 1.5 mL tube. 0.3 mL of acetonitrile was added to the supernatant and vortexed for 3 min, followed by centrifugation at 13000 rpm for 3 min. The supernatant was collected and analyzed by UPLC-MS/MS.

4.17. Molecular docking modeling

The crystal structure of MD-2 (PDB: 4G8A) was downloaded from the Protein Data Bank. Molecular docking calculations were performed using the Autodock Vina software 4.2. 3D structures of the active compound were generated and optimized using the AutoDock Tools 4.2, and were docked into the MD-2 protein. The relationship between the protein structure and the interaction force between the ligands was analyzed using the Discovery Studio 3.1 package. All the images were optimized and displayed using pymol (PyMOL v1.8.2.3; Schrödinger LLC).

4.18. Statistical analysis

All data were represented as mean ± SEM and were analyzed by one-way ANOVA. P-value less than 0.05 indicated that the difference was statistically significant. All experiments were repeated at least thrice.

Declaration of competing interest

The authors declare that they have no known competing financial interests or personal relationships that could have appeared to influence the work reported in this paper

Data availability

Data will be made available on request.

Acknowledgments

This study was funded in part with the funds provided by the National Natural Science Funding of China (21961142009, 82273791), Thailand Research Fund Grant (DBG6280006), Zhejiang Provincial Key Scientific Project (2021C03041), Scientific Research Starting Foundation in Wenzhou Medical University (QTJ21013), and Research Fund from the University of Chinese Academy of Sciences (WIUCASQD2020016).

Appendix A. Supplementary data

Supplementary data to this article can be found online at https://doi.org/10.1016/j.ejmech.2023.115289.

References

[1] N.R. Aggarwal, L.S. King, F.R. D'Alessio, Diverse macrophage populations mediate acute lung inflammation and resolution, Am. J. Physiol. Lung Cell Mol. Physiol. 306 (2014) L709–L725.
[2] A.V. Misharin, L. Morales-Nebreda, G.M. Mutlu, G.R. Budinger, H. Perlman, Flow cytometric analysis of macrophages and dendritic cell subsets in the mouse lung, Am. J. Respir. Cell Mol. Biol. 49 (2013) 503–510.
[3] B.T. Thompson, R.C. Chambers, K.D. Liu, Acute respiratory distress syndrome, N. Engl. J. Med. 377 (2017) 562–572.
[4] S.P. Luh, C.H. Chiang, Acute lung injury/acute respiratory distress syndrome (ALI/ARDS): the mechanism, present strategies and future perspectives of therapies, J. Zhejiang Univ. - Sci. B. 8 (2007) 60–69.
[5] R. Zhang, X. Wang, L. Ni, X. Di, B. Ma, S. Niu, C. Liu, R.J. Reiter, COVID-19: melatonin as a potential adjuvant treatment, Life Sci. 250 (2020), 117583.
[6] L. Liu, Q. Wei, Q. Lin, J. Fang, H. Wang, H. Kwok, H. Tang, K. Nishiura, J. Peng, Z. Tan, T. Wu, K.W. Cheung, K.H. Chan, X. Alvarez, C. Qin, A. Lackner, S. Perlman, K.Y. Yuen, Z. Chen, Anti-spike IgG causes severe acute lung injury by skewing macrophage responses during acute SARS-CoV infection, JCI Insight (2019) 4.
[7] Y.Q. He, C.C. Zhou, L.Y. Yu, L. Wang, J.L. Deng, Y.L. Tao, F. Zhang, W.S. Chen, Natural product derived phytochemicals in managing acute lung injury by multiple mechanisms, Pharmacol. Res. 163 (2021), 105224.
[8] M. Maes, E. Higginson, J. Pereira-Dias, M.D. Curran, S. Parmar, F. Khokhar, D. Cuchet-Lourenco, J. Lux, S. Sharma-Hajela, B. Ravenhill, I. Hamed, L. Heales, R. Mahroof, A. Soderholm, S. Forrest, S. Sridhar, N.M. Brown, S. Baker, V. Navapurkar, G. Dougan, J. Bartholdson Scott, A. Conway Morris, Ventilator-associated pneumonia in critically ill patients with COVID-19, Crit. Care 25 (2021) 25.
[9] A.S. Xi, M.G. Chang, E.A. Bittner, Rapid establishment of an ICU using anesthesia ventilators during COVID-19 pandemic: lessons learned, Crit. Care 24 (2020) 388.
[10] A.J. Boyle, R. Mac Sweeney, D.F. McAuley, Pharmacological treatments in ARDS; a state-of-the-art update, BMC Med. 11 (2013) 166.
[11] K. Dhaliwal, E. Scholefield, D. Ferenbach, M. Gibbons, R. Duffin, D.A. Dorward, A. C. Morris, D. Humphries, A. MacKinnon, T.S. Wilkinson, W.A. Wallace, N. van Rooijen, M. Mack, A.G. Rossi, D.J. Davidson, N. Hirani, J. Hughes, C. Haslett, A. J. Simpson, Monocytes control second-phase neutrophil emigration in established lipopolysaccharide-induced murine lung injury, Am. J. Physiol. Lung Cell Mol. Physiol. 186 (2012) 514–524.
[12] E. Azoulay, V. Lemiale, B. Mourvillier, M. Garrouste-Orgeas, C. Schwebel, S. Ruckly, L. Argaud, Y. Cohen, B. Souweine, L. Papazian, J. Reignier, G. Marcotte, S. Siami, H. Kallel, M. Darmon, J.F. Timsit, O.S. Group, Management and outcomes of acute respiratory distress syndrome patients with and without comorbid conditions, Intensive Care Med. 44 (2018) 1050–1060.
[13] A. Proudfoot, A. Bayliffe, C.M. O'Kane, T. Wright, A. Serone, P.J. Bareille, V. Brown, U.I. Hamid, Y. Chen, R. Wilson, J. Cordy, P. Morley, R. de Wildt, S. Elborn, M. Hind, E.R. Chilvers, M. Griffiths, C. Summers, D.F. McAuley, Novel anti-tumour necrosis factor receptor-1 (TNFR1) domain antibody prevents pulmonary inflammation in experimental acute lung injury, Thorax 73 (2018) 723–730.
[14] K.A. Brown, S.D. Brain, J.D. Pearson, J.D. Edgeworth, S.M. Lewis, D.F. Treacher, Neutrophils in development of multiple organ failure in sepsis, Lancet 368 (2006) 157–169.
[15] P. Fu, A.A. Birukova, J. Xing, S. Sammani, J.S. Murley, J.G. Garcia, D.J. Grdina, K. G. Birukov, Amifostine reduces lung vascular permeability via suppression of inflammatory signalling, Eur. Respir. J. 33 (2009) 612–624.
[16] J. Grommes, O. Soehnlein, Contribution of neutrophils to acute lung injury, Mol. Med. 17 (2011) 293–307.
[17] J.J. Farrell, L. Zhang, H. Zhou, D. Chia, D. Elashoff, D. Akin, B.J. Paster, K. Joshipura, D.T. Wong, Variations of oral microbiota are associated with pancreatic diseases including pancreatic cancer, Gut 61 (2012) 582–588.
[18] O.H. Voss, Y. Murakami, M.Y. Pena, H.N. Lee, L. Tian, D.H. Margulies, J.M. Street, P.S. Yuen, C.F. Qi, K. Krzewski, J.E. Coligan, Lipopolysaccharide-induced CD300b receptor binding to toll-like receptor 4 alters signaling to drive cytokine responses that enhance septic shock, Immunity 44 (2016) 1365–1378.
[19] L. Trifonov, V. Nudelman, M. Zhenin, E. Matsree, M. Afri, B. Schmerling, G. Cohen, K. Jozwiak, M. Weitman, E. Korshin, H. Senderowitz, A. Shainberg, E. Hochhauser, A. Gruzman, Structurally simple, readily available peptidomimetic 1-Benzyl-5-methyl-4-(n-octylamino)pyrimidin-2(1 H)-one exhibited efficient cardioprotection in a myocardial ischemia (MI) mouse model, J. Med. Chem. 61 (2018) 11309–11326.
[20] F.A. Facchini, L. Zaffaroni, A. Minotti, S. Rapisarda, V. Calabrese, M. Forcella, P. Fusi, C. Airoldi, C. Ciaramelli, J.M. Billod, A.B. Schromm, H. Braun, C. Palmer, R. Beyaert, F. Lapenta, R. Jerala, G. Pirianov, S. Martin-Santamaria, F. Peri, Structure-activity relationship in monosaccharide-based toll-like receptor 4 (TLR4) antagonists, J. Med. Chem. 61 (2018) 2895–2909.
[21] S.I. Yoon, M. Hong, I.A. Wilson, An unusual dimeric structure and assembly for TLR4 regulator RP105-MD-1, Nat. Struct. Mol. Biol. 18 (2011) 1028–1035.
[22] H.M. Kim, B.S. Park, J.I. Kim, S.E. Kim, J. Lee, S.C. Oh, P. Enkhbayar, N. Matsushima, H. Lee, O.J. Yoo, J.O. Lee, Crystal structure of the TLR4-MD-2 complex with bound endotoxin antagonist Eritoran, Cell 130 (2007) 906–917.
[23] J. Wilks, E. Lien, A.N. Jacobson, M.A. Fischbach, N. Qureshi, A.V. Chervonsky, T. V. Golovkina, Mammalian lipopolysaccharide receptors incorporated into the retroviral envelope augment virus transmission, Cell Host Microbe 18 (2015) 456–462.
[24] E. Patridge, P. Gareiss, M.S. Kinch, D. Hoyer, An analysis of FDA-approved drugs: natural products and their derivatives, Drug Discov. Today 21 (2016) 204–207.

[25] B.M. Bruel, A.W. Burton, Intrathecal therapy for cancer-related pain, Pain Med. 17 (2016) 2404–2421.
[26] H. Zhu, X. Gu, L. Xia, Y. Zhou, H. Bouamar, J. Yang, X. Ding, C. Zwieb, J. Zhang, A. P. Hinck, L.Z. Sun, X. Zhu, A novel TGFbeta trap blocks chemotherapeutics-induced TGFbeta1 signaling and enhances their anticancer activity in gynecologic cancers, Clin. Cancer Res. 24 (2018) 2780–2793.
[27] A. Ray Chaudhuri, Y. Hashimoto, R. Herrador, K.J. Neelsen, D. Fachinetti, R. Bermejo, A. Cocito, V. Costanzo, M. Lopes, Topoisomerase I poisoning results in PARP-mediated replication fork reversal, Nat. Struct. Mol. Biol. 19 (2012) 417–423.
[28] Q. Wu, F. Zhao, X. Zhu, Z. Zhou, D. Yang, Z. Xu, J. Li, Z. Qin, Design and synthesis of novel hydrocarbylidene nitrohydrazinecarboximidamides against aphids based on natural product galegine, Nat. Prod. Res. 35 (2021) 1484–1490.
[29] B.C. Goess, R.N. Hannoush, L.K. Chan, T. Kirchhausen, M.D. Shair, Synthesis of a 10,000-membered library of molecules resembling carpanone and discovery of vesicular traffic inhibitors, J. Am. Chem. Soc. 128 (2006) 5391–5403.
[30] L. Ji, L. Qu, C. Wang, W. Peng, S. Li, H. Yang, H. Luo, F. Yin, D. Lu, X. Liu, L. Kong, X. Wang, Identification and optimization of piperlongumine analogues as potential antioxidant and anti-inflammatory agents via activation of Nrf2, Eur. J. Med. Chem. 210 (2021), 112965.
[31] K. Liu, X. Zhao, X. Qi, D.L. Hou, H.B. Li, Y.H. Gu, Q.L. Xu, Design, synthesis, and biological evaluation of a novel dual peroxisome proliferator-activated receptor alpha/delta agonist for the treatment of diabetic kidney disease through anti-inflammatory mechanisms, Eur. J. Med. Chem. 218 (2021), 113388.
[32] Z. Sang, W. Pan, K. Wang, Q. Ma, L. Yu, Y. Yang, P. Bai, C. Leng, Q. Xu, X. Li, Z. Tan, W. Liu, Design, synthesis and evaluation of novel ferulic acid-O-alkylamine derivatives as potential multifunctional agents for the treatment of Alzheimer's disease, Eur. J. Med. Chem. 130 (2017) 379–392.
[33] G. Chen, Y. Zhang, X. Liu, Q. Fang, Z. Wang, L. Fu, Z. Liu, Y. Wang, Y. Zhao, X. Li, G. Liang, Discovery of a new inhibitor of myeloid differentiation 2 from cinnamamide derivatives with anti-inflammatory activity in sepsis and acute lung injury, J. Med. Chem. 59 (2016) 2436–2451.
[34] U. Werner, O. Seitz, I. Szelenyi, Stimulated elastase release from human leukocytes: influence of anti-asthmatic, anti-inflammatory and calcium antagonist drugs in vitro, Agents Actions 38 (1993) C112–C114.
[35] D. Gandhi, D.K. Agarwal, P. Kalal, A. Bhargava, D. Jangid, S. Agarwal, Synthesis, characterization and evaluation of novel benzothiazole clubbed chromene derivatives for their anti-inflammatory potential, Phosphorus, Sulfur, Silicon Relat. Elem. 193 (2018) 840–847.
[36] H. Song, G. Li, J. Ye, F. Wan, Y. Qian, Immunomodulating effects of cefodizime on Klebsiella pneumoniae-stimulated neutrophils, Immunobiology 209 (2004) 277–282.
[37] K. Tombácz, D. Mwangi, D. Werling, A.J. Gibson, Comparison of cellular assays for TLR activation and development of a species-specific reporter cell line for cattle, Innate Immun. 23 (2017) 329–335.
[38] Z. Chen, L. Zhang, J. Yang, L. Zheng, F. Hu, S. Duan, K.S. Nandakumar, S. Liu, H. Yin, K. Cheng, Design, synthesis, and structure-activity relationship of N-aryl-N'-(thiophen-2-yl)thiourea derivatives as novel and specific human TLR1/2 agonists for potential cancer immunotherapy, J. Med. Chem. 64 (2021) 7371–7389.
[39] Y. Xu, S. Chen, Y. Cao, P. Zhou, Z. Chen, K. Cheng, Discovery of novel small molecule TLR4 inhibitors as potent anti-inflammatory agents, Eur. J. Med. Chem. 154 (2018) 253–266.
[40] M. Oda, H. Yamamoto, M. Shibutani, M. Nakano, K. Yabiku, T. Tarui, N. Kameyama, D. Shirakawa, S. Obayashi, N. Watanabe, H. Nakase, M. Suenaga, Y. Matsunaga, M. Nagahama, H. Takahashi, H. Imagawa, M. Kurosawa, Y. Terao, M. Nishizawa, J. Sakurai, Vizantin inhibits endotoxin-mediated immune responses via the TLR 4/MD-2 complex, J. Immunol. 193 (2014) 4507–4514.
[41] Z. Liu, L. Chen, P. Yu, Y. Zhang, B. Fang, C. Wu, W. Luo, X. Chen, C. Li, G. Liang, Discovery of 3-(Indol-5-yl)-indazole derivatives as novel myeloid differentiation protein 2/Toll-like receptor 4 antagonists for treatment of acute lung injury, J. Med. Chem. 62 (2019) 5453–5469.
[42] Y. Zhang, Z. Liu, J. Wu, B. Bai, H. Chen, Z. Xiao, L. Chen, Y. Zhao, H. Lum, Y. Wang, H. Zhang, G. Liang, New MD2 inhibitors derived from curcumin with improved anti-inflammatory activity, Eur. J. Med. Chem. 148 (2018) 291–305.
[43] Y. Butt, A. Kurdowska, T.C. Allen, Acute lung injury: a clinical and molecular review, Arch. Pathol. Lab Med. 140 (2016) 345–350.
[44] P. Salovsky, V. Shopova, V. Dancheva, R. Marev, A. Pandurska, Enhancement of the pneumotoxic effect of cadmium acetate by ionizing radiation in the rat, Environ. Health Perspect. 101 (Suppl 2) (1993) 269–274.
[45] T. Cui, M. Miksa, R. Wu, H. Komura, M. Zhou, W. Dong, Z. Wang, S. Higuchi, W. Chaung, S.A. Blau, C.P. Marini, T.S. Ravikumar, P. Wang, Milk fat globule epidermal growth factor 8 attenuates acute lung injury in mice after intestinal ischemia and reperfusion, Am. J. Physiol. Lung Cell Mol. Physiol. 181 (2010) 238–246.
[46] M.A. Matthay, R.L. Zemans, The acute respiratory distress syndrome: pathogenesis and treatment, Annu. Rev. Pathol. 6 (2011) 147–163.
[47] X. Jin, C.J. Zheng, M.X. Song, Y. Wu, L.P. Sun, Y.J. Li, L.J. Yu, H.R. Piao, Synthesis and antimicrobial evaluation of L-phenylalanine-derived C5-substituted rhodanine and chalcone derivatives containing thiobarbituric acid or 2-thioxo-4-thiazolidinone, Eur. J. Med. Chem. 56 (2012) 203–209.
[48] A.H. Pang, K.D. Green, N.T. Chandrika, A. Garzan, A. Punetha, S.Y.L. Holbrook, M. J. Willby, J.E. Posey, O.V. Tsodikov, S. Garneau-Tsodikova, Discovery of substituted benzyloxy-benzylamine inhibitors of acetyltransferase Eis and their anti-mycobacterial activity, Eur. J. Med. Chem. 242 (2022), 114698.
[49] L. Zou, L. Sun, H. Zhang, W. Hui, Q. Zou, Z. Zhu, Identification, characterization, and quantification of impurities of safinamide mesilate: process-related impurities and degradation products, J. AOAC Int. 100 (2017) 1029–1037.
[50] J.S. Lee, H.K. Kim, S. Feng, M. Vendrell, Y.T. Chang, Accelerating fluorescent sensor discovery: unbiased screening of a diversity-oriented BODIPY library, Chem. Commun. 47 (2011) 2339–2341.
[51] J. Zhou, X. Shi, X. Dong, L. Sun, D. Shi, X. Liang, H. Xu, Tuning the molecular electronic structure and macroscopic aggregates of [2 + 2]-type H2- and Zn(II) porphyrins through meso-substituents, J. Coord. Chem. 75 (2022) 1230–1242.
[52] S. Xu, X. Xing, Y. Liu, H. Gao, A hemicyanine-based fluorescence probe for selective detection of CYP2D6 in living cells and tumor-bearing mice, Dyes Pigments 198 (2022), 109959.
[53] A.H. Martirosyan, S.P. Gasparyan, M.V. Alexanyan, G.K. Harutyunyan, H. A. Panosyan, R.F. Schinazi, Anti-human immunodeficiency activity of novel 2-arylpyrrolidine analogs, Med. Chem. Res. 26 (2017) 101–108.
[54] M. Kumar, P. Kumar Singh, S. Choudhary, O. Silakari, Hydantoin based dual inhibitors of ALR2 and PARP-1: design, synthesis, in-vitro and in-vivo evaluation, Bioorg. Chem. 129 (2022), 106108.
[55] M. Xi, J. Ge, X. Wang, C. Sun, T. Liu, L. Fang, Q. Xiao, D. Yin, Development of hydroxy-based sphingosine kinase inhibitors and anti-inflammation in dextran sodium sulfate induced colitis in mice, Bioorg. Med. Chem. 24 (2016) 3218–3230.
[56] S. Ghafary, Z. Najafi, M. Mohammadi-Khanaposhtani, H. Nadri, N. Edraki, N. Ayashi, B. Larijani, M. Amini, M. Mahdavi, Novel cinnamic acid-tryptamine hybrids as potent butyrylcholinesterase inhibitors: synthesis, biological evaluation, and docking study, Arch. Pharm. 351 (2018), 1800115.
[57] J. Zhu, H. Yang, Y. Chen, H. Lin, Q. Li, J. Mo, Y. Bian, Y. Pei, H. Sun, Synthesis, pharmacology and molecular docking on multifunctional tacrine-ferulic acid hybrids as cholinesterase inhibitors against Alzheimer's disease, J. Enzym. Inhib. Med. Chem. 33 (2018) 496–506.
[58] K.S. Raju, G. Sabitha, First total synthesis of Brevipolide N and total synthesis of Brevipolide M, Tetrahedron Lett. 59 (2018) 4213–4215.